SEMMELWEIS EGYETEM

DOKTORI ISKOLA

Ph.D. értekezések

3357.

KORMOSNÉ VARRÓ NIKOLETT

A gyógyszerészeti tudományok korszerű kutatási irányai

című program

Programvezető: Dr. Antal István, egyetemi tanár

Témavezetők: Dr. Mándity István, egyetemi docens

Synthesis and investigation of modified peptides

PhD thesis

Nikolett Kormosné Varró

Semmelweis University Doctoral School

Doctoral School of Pharmaceutical Sciences

Supervisor: István Mándity, Ph.D.
Official reviewers: Krisztina Ludányi, Ph.D
Ildikó Szabó, Ph.D

Head of the Complex Examination Committee: István Antal, professor

Members of the Complex Examination Committee: Tamás Beke-Somfai, Ph.D
Krisztina Ludányi Ph.D

Budapest
2025

List of Abbreviations

ACHC	[*1R,2R*]-2-aminocyclohexanecarboxylic acid
ACPC	[*1S,2S*]-2-aminocyclopentanecarboxylic acid
AI	artificial intelligence
APIs	active pharmaceutical ingredients
CD	circular dichroism
CD_3OH	1,1,1-trideuteromethanol
CF	continuous-flow
CF-SPPS	continuous-flow solid-phase peptide synthesis
COSY	correlation spectroscopy
CPME	cyclopentyl methyl ether
DBU	1,8-diazabicyclo[5.4.0]undec-7-ene
DCC	*N,N*-dicyclohexylcarbodiimide
DCM	dichloromethane
DIC	*N,N'*-diisopropylcarbodiimide
DIPEA	*N,N*-diisopropylethylamine
DLS	dynamic light scattering
DMF	*N,N*-dimethylformamide
DMSO	dimethyl sulfoxide
DNA	deoxyribonucleic acid
D_2O	deuterium oxide
DTT	DL-dithiothreitol
ECD	electronic circular dichroism
Fmoc	fluorenylmethoxycarbonyl
FT-IR	Fourier-transform infrared spectroscopy
GSK	Glaxo Smith Kline – solvent selection guide
HATU	1-[bis(dimethylamino)methylene]-1*H*-1,2,3-triazolo[4,5-*b*]pyridinium 3-oxide hexafluorophosphate
HIV	Human Immunodeficiency Virus
HOAt	1-hydroxy-7-azabenzotriazole
HPLC	high-performance liquid chromatography

HPLC-MS	high-performance liquid chromatography-mass spectrometry
MCT	mercury-cadmium-telluride
MeOH	methanol
ML	machine learning
MQ water	Milli-Q water
NMR	nuclear magnetic resonance spectroscopy
OxymaPure	ethyl (hydroxyimino)cyanoacetate
PATs	process analytical technologies
PBS	phosphate-buffered saline
PC	propylene carbonate
PEEK	polyetheretherketone
PNA	nucleic acid analogs
ROESY	rotating-frame nuclear Overhauser effect spectroscopy
RNA	ribonucleic acid
RP-HPLC	reverse-phase high-performance liquid chromatography
SPPS	solid-phase peptide synthesis
TEM	transmission electron microscopy
TFA	trifluoroacetic acid
TIPS	tris(1-methylethyl)silane
TOCSY	total correlation spectroscopy
2-Me THF	2-methyltetrahydrofuran

1. Introduction

1.1. Foldamer

Biopolymers, including nucleic acids (RNA and DNA), proteins, and peptides, are fundamental to the structure and function of living organisms. (1) Proteins and peptides are composed of amino acids, containing 20 different types of α-L amino acids, some of which are essential. (2) Beyond naturally occurring amino acids, scientists have developed synthetic non-natural amino acids and peptide-like compounds in laboratory settings, expanding their applications in research, (3) medicine, (4) and biotechnology. (5) These artificially synthesized molecules enable the study of biological activities, (6, 7, 8) the design of targeted therapies, (9, 10, 11) and the development of novel treatments for various diseases. (12, 13, 14)

Peptides play an essential role in physiological processes such as hormone regulation, (15, 16) immune response, (17, 18) and cell signaling. (19, 20) Furthermore, they are utilized in various applications, including cargo delivery systems, (20) hydrogel nanofibers, (21) and drug development. (21) Artificially produced peptides and proteins can mimic endogenous biological substances, enhancing their functional potential. Additionally, numerous engineered peptides, and peptoids have been successfully synthesized to replicate biopolymer structures and properties. (8)

The stability and structural behavior of peptide derivatives have been a subject of extensive research. From the 20th century more and more research has focused on the structure (22, 23, 24) and stability of β-peptides compared to α-peptides. (25, 26, 27) Subsequent studies examined β-peptides with various side chains, (28, 29) along with γ- and δ-peptides, highlighting their structural diversity *(Figure 1.)*. (30) Alternative backbone modifications, (31) including the replacement of amide bonds with ureas, hydrazides, or hydroxyamides, have also been explored, resulting in stable folded structures. (32) These synthetic peptides are often designed to mimic biological systems and are referred to as "biotic" molecules. (33, 34, 35)

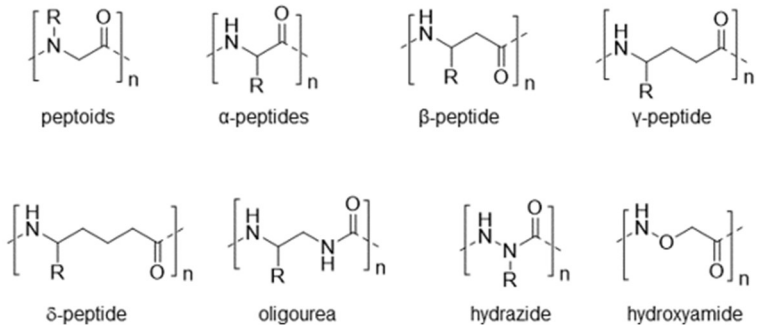

1. Figure Examples of peptide structures

Foldamers represent a distinctive class of artificially synthesized, self-assembling polymers that incorporate non-natural systems. (36, 37) Their secondary structure can be pre-designed, enabling the creation of biomimetic molecules with specific functionalities. (38, 39) These polymers exhibit a propensity to fold into various conformations, including helices, sheets, linear strands, and turns. (40, 41) The stability of their ordered conformations is governed by non-covalent interactions such as hydrogen bonding, hydrophobic effects, electrostatic forces, and van der Waals interactions, which occur between non-adjacent monomer units. (35) This structural adaptability and stability make foldamers valuable in the development of artificial molecular architectures with potential applications in biomimetic research and material sciences. (42)

1.1.1. β-peptides

β-Peptides, a significant subclass of foldamers, are composed of β-amino acids and can be efficiently synthesized through established pathways. Structurally, they resemble α-peptides but possess key differences that enhance their stability against metabolic degradation (43, 44) and proteolytic enzymes, as well as improve membrane permeability. (45) The presence of an additional methylene group between peptide bonds enables stabilizing intramolecular hydrogen bonding, contributing to their conformational diversity. (46, 47) β-Peptides can be mono- or di-substituted and may form cyclic ring structures, with chirality further enriching their structural versatility. (48, 49)

Their structural integrity stems from β-amino acids, which differ from α-amino acids by positioning the amino group on the β-carbon. This alteration affects the oligomer's secondary structure and interactions with biological targets. (50, 51, 52) A well-studied conformation is the 12-helix, stabilized by intramolecular hydrogen bonds, such as that found in foldamers composed of [1*S*,2*S*]-2-aminocyclopentanecarboxylic acid.

Modifications in side chains, including cyclic residues and unnatural amino acids, enhance stability and hydrophobic interactions. (53, 54)

β-Peptide foldamer structures are shaped by various factors, including side-chain substitutions, backbone stereochemistry, (55, 56) and non-covalent interactions such as steric repulsion, electrostatic forces, and solvophobic effects. (57, 58) The inherent flexibility of the β-amino acid backbone allows for precise tuning of foldamer properties, facilitating diverse functional applications in biomimetics and material sciences.

1.1.2. Function of β-peptide foldamers

β-Peptide foldamers mimic natural peptides and exhibit antimicrobial, antiviral, and anticancer properties, making them valuable for therapeutic applications due to their resistance to enzymatic degradation. (59, 60) Their structural features (61) enable them to competitively inhibit viral entry by mimicking host receptor domains, particularly in HIV (62, 63) and influenza research. Additionally, their rigidity and tunable side chains allow for the development of selective enzyme inhibitors targeting proteases and kinases with high specificity. β-Peptides also disrupt protein-protein interactions in disease-related signaling pathways, facilitating advancements in biomolecular recognition and catalysis. These characteristics position β-peptide foldamers as promising tools in drug development and biomedical research. (64, 65)

1.1.3. Importance of β-peptide foldamers in drug development

Foldamers are versatile molecules with broad applications in drug design, (46, 66) material science, nanotechnology, (67) and catalysis. (68, 69) Their ability to emulate peptide structures while maintaining biocompatibility makes β-peptide foldamers particularly valuable in therapeutics, enabling targeted drug delivery and immunomodulation. These foldamers have been integrated into nanostructures such as vesicles and micelles, enhancing pharmacokinetics and cellular uptake. (70, 71)

Beyond drug development, foldamers play a crucial role in nanotechnology by self-assembling into nanocarriers and responsive materials. Their adaptability allows for the creation of molecular sensors, diagnostic tools, and environmental monitors, with potential use in detecting cancer biomarkers or pollutants. Structural modifications and side-chain diversity enable fine-tuning of their properties, expanding their utility in biomolecular recognition and therapeutic applications. (72)

Recent advances highlight β-peptide foldamers as promising candidates for disrupting key protein interactions, such as those involved in tumor suppression. (73, 74) Their stability and ability to traverse biological membranes further position them as effective drug delivery systems and molecular therapeutics. (75, 76)

1.1.4. Future directions and challenges

As the field progresses, continued exploration of the design and optimization of β-peptide foldamers is essential for translating their unique properties into clinical applications. Challenges remain regarding the large-scale synthesis, characterization, and delivery of these compounds. Furthermore, comprehensive biological evaluations of the pharmacokinetics and potential toxicities attributed to β-peptide foldamers are necessary to ensure their safety and efficacy in therapeutic contexts.

Efforts are underway to enhance the functional scope of β-peptide foldamers through strategic modifications that improve their cellular uptake and modulatory properties against diverse biological targets. Advances in computational design tools and synthetic methodologies will aid in refining these foldamer structures to develop optimized therapeutic agents. (77, 78)

In summary, β-peptide foldamers represent a new frontier in peptide chemistry with immense potential for therapeutic applications. Their unique structural characteristics facilitate the emulation of biologically relevant conformations while offering enhanced stability and functionality. A significant number of synthesis methods are available for the production of peptides and foldamers, each of which has its own advantages and disadvantages. As research advances, these foldamers may play pivotal roles in drug discovery, biomolecular targeting, and the development of novel therapeutic modalities. (79)

1.2. Continuous-flow synthesis technologies

Continuous-flow synthesis technologies represent a significant advancement in the field of chemical synthesis, offering numerous advantages over traditional batch processes. This innovative approach enables the continuous introduction of reagents into a reaction pathway, fostering improved reaction conditions, automation, and scalability. (80, 81) As industries seek to enhance efficiency, reduce waste, and meet economic and environmental sustainability standards, continuous-flow methodologies have garnered

increasing attention across various domains, including pharmaceuticals, (82) materials science, and specialty chemicals. (83, 84)

1.2.1. Structure and mechanism of continuous-flow systems

Continuous-flow reactors, consisting of interconnected microreactors and tubing systems, offer significant improvements over conventional batch processes by enabling precise control over reaction conditions such as temperature, pressure, and residence time. (85) Their integration with real-time monitoring tools, including process analytical technologies (PATs), ensures consistent product quality and enhances operational safety. The modular and scalable nature of these systems facilitates the efficient transition from laboratory research to industrial production. (86)

Microreactors, a key implementation of continuous-flow technology, provide enhanced heat and mass transfer due to their high surface area-to-volume ratio, allowing for rapid thermal equilibration and improved reaction selectivity. (87, 88) Their versatility extends to various reaction types, including liquid-liquid, gas-liquid, and solid-liquid processes, making them highly applicable to homogeneous catalysis and multiphase reactions. Additionally, continuous-flow processing aligns with green chemistry principles by reducing solvent usage, waste generation, and energy consumption. (89)

By offering superior scalability, automation potential, and environmental benefits, continuous-flow reactors represent a transformative approach to chemical synthesis, supporting advancements in drug development, material science, and process optimization. (90) Their ability to intensify reactions while maintaining safety and efficiency positions them as a critical technology for modern chemical engineering. (91, 92)

1.2.2. Advantages of continuous-flow synthesis

Continuous-flow synthesis offers numerous advantages, including improved safety, enhanced reaction efficiency, and reduced environmental impact. By operating in a closed system, these reactors minimize exposure to hazardous materials and mitigate risks associated with highly reactive intermediates, such as toxic or thermally unstable reagents. Their precise control over residence time and reaction conditions enables the safe execution of exothermic processes and traditionally high-risk reactions, such as nitration and diazotization. (93)

The integration of real-time monitoring tools, including infrared and Raman spectroscopy, enhances process control and ensures consistent product quality. Continuous-flow systems facilitate higher yields and selectivity through automated feedback mechanisms, optimizing reaction parameters. (94) Moreover, steady-state operation eliminates batch-to-batch variability, improving reproducibility and efficiency, particularly in multistep syntheses. (95)

Automation and high-throughput experimentation further accelerate reaction optimization and process development. The modular nature of continuous systems supports iterative synthesis and seamless scalability, allowing for integration with robotic platforms and machine learning-driven self-optimizing workflows. Their ability to reduce waste aligns with green chemistry principles, promoting sustainable manufacturing through solvent minimization, in-line purification, and improved atom economy.(96) As continuous-flow technology advances, its applications in chemical synthesis, drug development, and industrial processes continue to expand, reinforcing its role in modern green chemistry initiatives. (97)

1.2.3. Application in industry

Continuous-flow synthesis has become integral to pharmaceutical and materials science research, enabling efficient production of active pharmaceutical ingredients (APIs) and advanced materials. In drug development, continuous-flow methods facilitate the synthesis of complex molecules, such as oseltamivir and stavudine, while minimizing intermediate purification, reducing processing time, and improving solvent efficiency. (98, 99) The enhancement of stereoselective drug production is achievable through the optimisation of reaction conditions.

Recent advancements integrate automation and machine learning into continuous-flow systems, allowing self-optimizing synthesis and high-throughput screening, which accelerates process development and scalability. The technology addresses traditional drug development challenges, such as hazardous reagent handling, reproducibility, and environmental sustainability, leading to broader adoption in commercial pharmaceutical manufacturing.

In materials science, continuous-flow synthesis enables rapid fabrication of nanoparticles and microporous crystalline materials, benefiting applications in catalysis, energy storage, and biomedical engineering. Microfluidic platforms improve control over

particle size distribution and morphology, enhancing efficiency compared to batch processes. The scalability and precision of continuous-flow systems support the development of functional materials with tailored physicochemical properties, reinforcing their significance in modern chemical engineering. (100)

1.2.4. Challenges and future directions

Despite its numerous advantages, continuous-flow synthesis faces challenges in scaling from laboratory to industrial settings, where maintaining efficiency in larger reactors can be difficult due to constraints in geometry, pressure drop, and throughput capacity. Additionally, specialized equipment and interdisciplinary expertise are required for industrial implementation, increasing costs and complexity, particularly for smaller enterprises. Regulatory standards, especially in pharmaceutical applications, further complicate adoption, necessitating robust analytical technologies to ensure consistency in product quality. (101)

Ongoing research explores solutions such as modular reactor designs, hybrid batch-flow systems, and predictive digital modeling, which aim to facilitate wider adoption of continuous-flow technology. Future advancements are expected to focus on integrating catalysis and in-line purification methods, enhancing sustainability and efficiency. Furthermore, artificial intelligence (AI) and machine learning are playing a growing role in optimizing reaction conditions, enabling real-time process adjustments and improving operational efficiency. (102)

These technological innovations hold transformative potential for chemical manufacturing, making continuous-flow synthesis more scalable, accessible, and sustainable. (103) As advancements continue, its applications in pharmaceuticals, advanced materials, and green chemistry will expand, solidifying its role in modern chemical engineering. (104)

1.3. Solid-phase peptide synthesis

Solid-phase peptide synthesis (SPPS) is a technique pioneered by R. Bruce Merrifield in the 1960s, which revolutionized peptide chemistry by enabling the rapid and efficient synthesis of peptides. (105, 106) This method synthesizes polypeptides on an insoluble solid support by sequentially adding amino acids. SPPS allows straightforward manipulation whether at a small scale in laboratories or for large-scale industrial applications. (107, 108) Its efficiency and ease of use have solidified SPPS as the

preferred method for producing therapeutic peptides (109) and biopharmaceuticals. (110, 111)

1.3.1. Mechanism of solid-phase peptide synthesis

Peptide elongation was created by Fmoc strategy, where amino acids are sequentially added and deprotected using coupling reagents such as HATU or DIC. Additives like Oxyma Pure or HOAt are used to improve coupling efficiency and suppress racemization, particularly for sterically hindered residues. (112) Automation of this process has significantly increased reproducibility and throughput, making SPPS the preferred method for peptide synthesis in research and pharmaceutical applications. (113)

Final peptide cleavage occurs using strong acids like trifluoroacetic acid (TFA), often combined with scavengers to minimize side reactions. The cleavage efficiency depends on resin type, protecting groups, and cocktail composition. Small-scale test cleavages and analytical techniques such as HPLC and mass spectrometry are employed to ensure peptide integrity and purity. Continuous advancements in cleavage protocols have improved peptide yield and quality, reinforcing SPPS as a fundamental technique in synthetic peptide chemistry. (114)

1.3.2. Advantages of solid-phase peptide synthesis

Automation plays a crucial role in SPPS, ensuring reproducibility and scalability for large-scale production. Advanced technologies, including microwave-assisted synthesis, have improved coupling efficiency and reduced reaction times, enabling the synthesis of longer and more complex peptides. Additionally, SPPS supports the incorporation of non-natural amino acids and post-translational modifications, expanding its applications in drug development and biomedical research. (115)

Recent innovations, such as orthogonal protecting group strategies and real-time monitoring systems, have further enhanced SPPS, allowing for the synthesis of peptide libraries and multifunctional conjugates. The automation of SPPS accelerates drug discovery timelines and improves process robustness, reinforcing its role as a fundamental technique in peptide-based therapeutic development. The continued evolution of SPPS, including flow-based and high-throughput technologies, promises further advancements in peptide synthesis efficiency and versatility.

1.3.3. New directions in solid-phase peptide synthesis

Solid-phase peptide synthesis (SPPS) has advanced significantly, yet challenges remain, particularly in synthesizing longer peptides, incorporating non-natural amino acids, and optimizing reaction conditions to improve efficiency and reduce side reactions. (116, 117) Ongoing innovations address these challenges, particularly through green chemistry initiatives, improved coupling strategies, and automation.

Efforts to enhance sustainability in SPPS include replacing traditional solvents such as DMF and DCM with environmentally friendly alternatives like 2-methyltetrahydrofuran (2-MeTHF) and cyclopentyl methyl ether (CPME), which maintain synthesis efficiency while reducing environmental impact. Additionally, approaches such as reduced solvent volumes, recycling, and aqueous-phase coupling align with green chemistry principles, making peptide synthesis more sustainable. (118, 119)

Optimization of coupling strategies has led to the development of highly reactive reagents, such as uronium and phosphonium compounds, which improve reaction rates and suppress racemization. Advanced methods, including real-time monitoring, double coupling strategies, and microwave-assisted SPPS, enhance synthesis efficiency and purity, especially for complex sequences. (120) Microwave irradiation accelerates coupling and deprotection steps, enabling the high-throughput synthesis of peptide libraries with reduced cycle times. (121, 122)

Further advancements include traceless linkers, which simplify peptide purification by eliminating resin residues, and the integration of SPPS with continuous-flow systems, improving scalability and real-time reaction monitoring. (123) These approaches enhance automation and process control, paving the way for more efficient and cost-effective peptide production. (124, 125)

As research continues, SPPS is evolving into a more sustainable, precise, and scalable platform for peptide synthesis, supporting advancements in drug development and biomedical applications. Its integration with emerging technologies ensures its continued prominence in pharmaceutical innovation.

2. Objectives

During the course of my doctoral research, I sought to synthesise artificial self-assembly foldamers, undertake their structural analysis, automate their synthesis, increase the volume of synthesis and enenhance their environmental sustainability.

As a preliminary step, I synthesised a self-assembly molecule composed of β-amino acids by solid phase peptide synthesis. Then, I purified the resulting peptide by RP-HPLC.

In order to obtain further information about the structure of the synthesised peptide, a range of NMR measurements (COSY, TOCSY, ROESY), ECD and FT-IR were performed. These studies indicated that a well-defined structure had been successfully formed.

The subsequent step was to automate the synthesis, which initially proved challenging due to the coupling of β-amino acids. Consequently, the conditions for the automated synthesis had to be defined with the most optimal conditions. This was initially done with shorter peptide chains composed of α-amino acids, and then longer chains were produced with increasing chain lengths and better yields. The parameters necessary for successful synthesis had been established. The experiment proved successful in a continuous-flow, automated system.

The primary challenge was to enhance the environmental sustainability of the synthesis. The solvent utilised in the process exhibited the greatest environmental impact, prompting the investigation of alternatives with a reduced environmental footprint. Research has demonstrated propylene carbonate to be the most prevalent green solvent in recent years, thus prompting the replacement of DMF with this alternative. This substitution yielded a synthesis that operated flawlessly, with no decline in yield and no deterioration in material quality. Consequently, it can be concluded that the transformation of the reaction into a more environmentally sustainable process was successful.

3. Methods

3.1. Peptide synthesis

3.1.1. Solid phase peptide synthesis in a Merrifield-glass

With Fmoc chemistry, the peptide chains were elongated on Tentagel R RAM resin (0.20 mmol g^{-1}). First, 3 equivalents of Fmoc-protected amino acid, 2.5 equivalents of the coupling agent ethyl cyanoglyoxylate-2-oxime (OxymaPure) and 3 equivalents of *N,N*-dicyclohexylcarbodiimide (DCC) were used in *N,N*-dimethylformamide (DMF) as solvent with shaking for 2 h. After the coupling step, the resin was washed 3 times with DCM, once with MeOH and 3 times with DCM. Deprotection was performed with 2% 1,8-diazabicyclo[5.4.0]undec-7-ene (DBU) and 2% piperidine in DMF in two steps, with reaction times of 5 and 15 min. The resin was washed with the same solvents as described previously. The cleavage was performed with TFA/water/TIPS/DTT (95:2:2:1) at 0 °C for 2 h.

3.1.2. Continuous flow solid phase peptide synthesis

Peptide chains were extended on a Tentagel R RAM resin (0.20 mmol g^{-1}). For CF experiments, a modular CF apparatus was assembled, consisting of a cylindrical PEEK column (with internal dimensions of 250×4 mm) filled with the resin (350 mg), a semi-preparative pump (JASCO PU-4086), an HPLC autosampler (JASCO AS-4150), a column oven (JASCO CO-4060), two line-selecting valve units (JASCO HV-4380), and a backpressure regulator. A coupling mixture, consisting of 1.5 equivalents of Fmoc-protected β-amino acid and 1.5 equivalents of OxymaPure as coupling reagent dissolved in DMF and 1.5 equivalents of DIC, was mixed by the autosampler. The coupling mixture has been prepared immediately before the coupling reaction by the autosampler of the reactor. Coupling reactions were carried out at the optimized reaction conditions, 60 bar pressure, 65 °C temperature, and 0.2 mL min^{-1} flow rate. For Fmoc deprotection the solution of 2 mL of 2% DBU 2% piperidine in DMF has been used. Between two chemical steps DMF was used for washing for 5 min. The cleavage was performed with the same method, TFA/water/TIPS/DTT (95:2:2:1) at 0 °C for 2 h in a round-bottom flask.

3.2. Structure investigations

3.2.1. Circular dichroism (CD) spectroscopy

CD spectra were measured on a Jasco J-1500 spectropolarimeter at 25°C in a 0.1 cm path length regtangular quartz cuvette (Hellma, Plainview, NY) in a continuous scanning mode between 190 and 250 nm at a rate of 50nm min^{-1} , with a data pitch of 0.5 nm, a response time of 4 s, a 1 nm bandwidth and 3 times accumulation for each sample. The baseline spectrum recorded with only the solvent was subtracted from the raw data. The concentration of the sample solutions in ultrapure water, methanol and PBS was 1 mM. Molar circular dichroism is given in molar ellipticity.

3.2.2. Fourier-transform infrared spectroscopy (FT-IR)

A Varian 2000 FT-IR Scimitar spectrometer (Varian Inc., Palo Alto, CA) was used for FT-IR spectroscopic measurements. The spectrometer is fitted with a liquid nitrogen-cooled mercury-cadmium-telluride (MCT) detector with a "Golden Gate" single reflection diamond ATR accessory (Specac Ltd., Orpington, U.K.). On the diamond ATR surface, 3 µL of the sample was mounted and spectrum was accumulated (2 cm -1 resolution and 64 scans) for the dry film after gradual evaporation of the buffered solvent under ambient conditions. ATR correction for every data acquisition, buffer subtraction and baseline corrections were performed. The GRAMS/32 software package (Galactic Inc.) was used for all spectral manipulations.

3.2.3. Nuclear magnetic resonance (NMR)

NMR measurements for signal assigment were carried out on a Bruker Avance III 500 MHz spectrometer equipped with a cryo probe head. Peptide samples (4 mM) were prepared in H_2O/D_2O 90:10 v/v, DMSO-d_6 or CD_3OH and transferred into 5 mm NMR sample tubes. For the ROESY spinlock, a mixing time of 300 ms was used; the number of scans was 16 and roesyesgpph or roesyph.2 (DMSO-d_6) pulse sequence was applied. The TOCSY measurement was performed with the mlevesgpph or mlevph (DMSO-d_6) sequence, with a mixing time of 150 ms; the number of scans was 16. For all 2D spectra, 4k time domain points and 512 increments were applied. T2 relaxation experiments were carried out by cpmg_esgp2d or cpmg (DMSO-d_6) pulse sequence; the relaxation delays were incremented in the following order: 1, 2, 4, 8, 16, 32, 64, 128, 256, 512, and 1024 ms.

The NH/ND exchange was recorded on a Varian Mercury 400 spectrometer equipped with ATB PFG probe head. The samples were prepared in 4 mM concentration in CD_3OD and transferred into standard 5 mm NMR sample tubes. The recording was started 10 minutes after complete solubilization. The ^1H spectra were recorded using 64 scans with 45 degree pulse and 5 s relaxation delay.

3.3. Particle size measurement

3.3.1. Dynamic light scattering (DLS)

DLS measurements can provide information about the size distribution profile of matter in solution. The peptides were dissolved in MQ water to a concentration of 4 mM. DLS measurements were performed at 25°C on a Litesizer 500 (Anton Paar, Hamburg, Germany) equipped with a He-Ne laser (backscattered detector fixed at 175°, side scatter 90° detector angle, front scatter 15°detector angle). The correlation function and distribution of the apparent hydrodynamic diameter (d_h) over the scattered intensity of the samples were determined on the basis of 3×10 scans.

3.3.2. Transmission electron microscopy (TEM)

TEM measurements can give information about the morphology of the matter. The peptides were dissolved in water to a concentration of 1 mM and the solution was sonicated for 5 min. Drops of 5 μL of solutions were placed onto the specimen holder, 200-mesh copper grid with a support film made of 01700-F formvar (Ted Pella, Inc. USA) and dried on the air on 25 °C for 10 min. Specimens were studied with a MORGAGNI 268D (FEI, Endhoven, The Netherlands) transmission electron microscope operating at 80 kV and equipped with a Quemesa 11-megapixel bottom-mounted CCD camera (Emsis GmbH, Germany). Images were taken with a view system, at magnifications of ×10000 and ×8000 and analyzed on the iTEM analysis platform (RADIUS 2.1 Acquisition and Control Software; EMSIS Gmbh, Germany).

4. Results

4.1. Betain-conjugated foldamers

Two principal archetypes of β-peptide helices have been extensively characterized in three dimensions: the right-handed H12 helix, formed by homochiral homooligomers of [1*S*,2*S*]-2-aminocyclopentanecarboxylic acid (ACPC), and the right-handed H10 helix, formed by the homochiral tetramer of [1*R*,2*R*]-2-aminocyclohexanecarboxylic acid (ACHC). In contrast, strand-like conformations are exemplified by previously reported alternating heterochiral homooligomers composed of [1*S*,2*S*]-ACPC and [1*R*,2*R*]-ACPC residues.

In the present study, these oligomeric systems were functionalized with an N-terminal betaine moiety. Specifically, we synthesized a betaine-conjugated homochiral pentamer of [1*S*,2*S*]-ACPC, a betaine-conjugated tetramer of [1*R*,2*R*]-ACHC, and a betaine-conjugated alternating heterochiral homooligomer comprising [1*S*,2*S*]-ACPC and [1*R*,2*R*]-ACPC residues. The molecular structures of the synthesized betaine-functionalized oligomers are depicted in *Figure 2*.

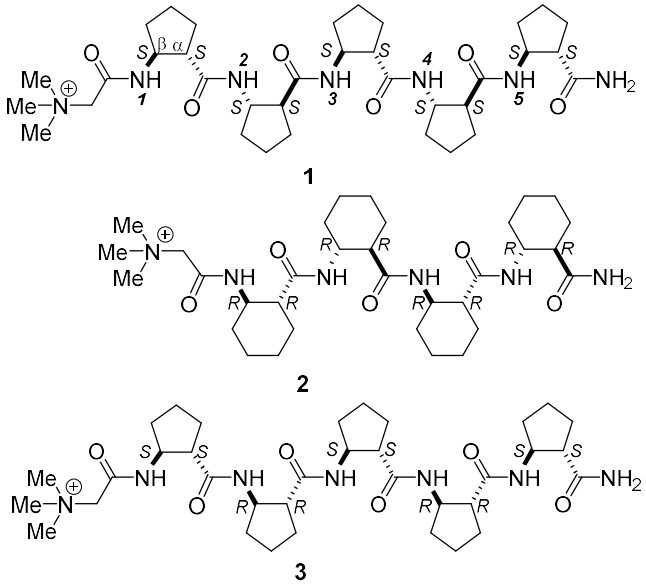

2. Figure The chemical structures of betaine-conjugated foldamers (126)

4.1.1. Synthesis of foldamers

The initial synthesis of compounds **1–3** was attempted using conventional SPPS protocols. However, the incorporation of betaine, a sterically demanding moiety bearing a quaternary ammonium group, proved unsuccessful under these conditions, as the target products could not be isolated. To address this limitation, continuous-flow solid-phase

peptide synthesis (CF-SPPS) was employed. This method enables efficient coupling with minimal excess of amino acid reagents while ensuring complete reaction conversion. Although CF-SPPS has previously been applied to the synthesis of β-peptides, its utility for the conjugation of bulky betaine groups to sterically hindered β-amino acids had not been demonstrated. Under optimized CF-SPPS conditions, compounds **1–3** were successfully synthesized, yielding crude products with purities exceeding 96% and isolated yields greater than 91%.

4.1.2. Structure investigation

4.1.2.1. Results of NMR investigation

The three-dimensional conformations of compounds **1–3** were initially investigated through NH/ND exchange experiments, monitored via a series of 1H NMR spectra recorded in CD_3OD at a concentration of 4 mM and a temperature of 297 K. For compound **1**, the time-dependent attenuation of NH signal intensities indicated significant protection from solvent exchange, consistent with intramolecular hydrogen bonding (*Figure 3*).

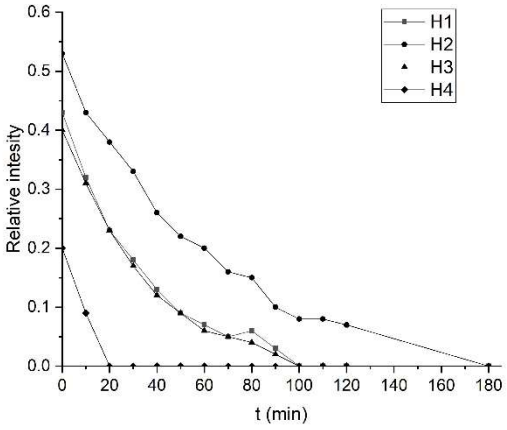

3. Figure Time dependence of the NH/ND exchange for 4-mM solutions of 1 in CD_3OD (126)

Notably, the amide proton at the C-terminus underwent rapid exchange upon dissolution, whereas other NH signals persisted for longer durations. The slowest exchange was observed for NH2, located centrally within the helix, suggesting substantial shielding. NH1 and NH3 also exhibited slow exchange, with the latter expected due to its central position. The unexpectedly slow exchange of NH1 is likely attributable to steric shielding by the adjacent bulky betaine moiety. In contrast, NH4 exchanged more rapidly, and NH5 was lost immediately upon dissolution.

In the case of compound **2**, significantly slower exchange kinetics were observed. Over a two-week period, only 5–10% exchange occurred, and complete exchange was not achieved even after two months. These findings do not support the formation of an H10 helix; rather, they are indicative of an H14 helical fold and suggest potential self-association.

For compound **3**, all amide protons exchanged immediately upon dissolution, consistent with an extended, strand-like conformation.

To obtain high-resolution structural information, additional NMR experiments — including COSY, TOCSY, and ROESY — were conducted in CD_3OD, DMSO, and aqueous solution (90% H_2O/10% D_2O) at 4 mM concentration and 297 K. Complete backbone proton assignments were achieved for compounds **1** and **2**. Long-range NOE interactions, characteristic of helical β-peptide secondary structures, were identified and are presented in *Figure 4*.

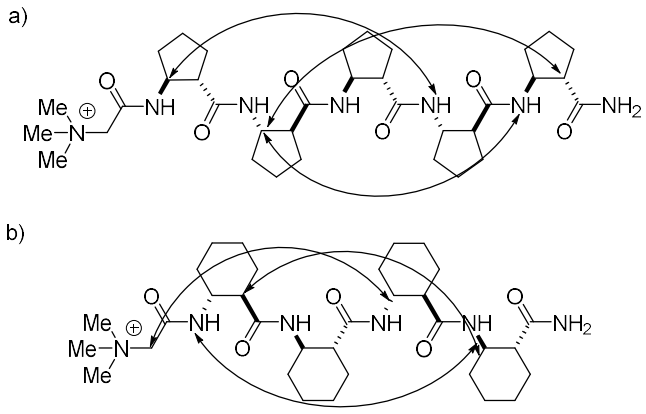

4. Figure Long-range NOE interactions for 1 (a) in DMSO-d6, and for 2 (b) found in DMSO-d6, CD_3OH or water (90% H_2O + 10% D_2O) (126)

For compound **1**, NOE cross-peaks such as HN(4)–Hβ(1), HN(5)–Hβ(2), and Hα(5)–Hβ(2) were observed in all solvents tested, confirming the formation of an H12 helix. These interactions were consistent across methanol, water, and even the chaotropic solvent DMSO, indicating that the helical structure is retained upon betaine conjugation. In contrast, compound **2** exhibited a distinct NOE pattern, including HN(1)–Hβ(4), Hα(1)–Hβ(4), and CH_2(betaine)–Hβ(3), which are indicative of an H14 helical conformation. These results suggest that the presence of the betaine moiety alters the preferred secondary structure, favoring H14 over the previously reported H10 helix.

For compound **3**, poor signal dispersion precluded complete backbone assignment and the identification of long-range NOEs. This lack of dispersion supports the presence of a

strand-like conformation. Nevertheless, the incorporation of the charged quaternary ammonium group from the betaine moiety enhanced solubility in CD_3OD, DMSO, and aqueous solution at 4 mM, thereby enabling further structural characterization.

4.1.2.2. ECD

To further substantiate the structural characterization of the synthesized compounds, electronic circular dichroism (ECD) spectroscopy was performed in methanol and aqueous solutions at a concentration of 1 mM and ambient temperature (*Figure 5*).

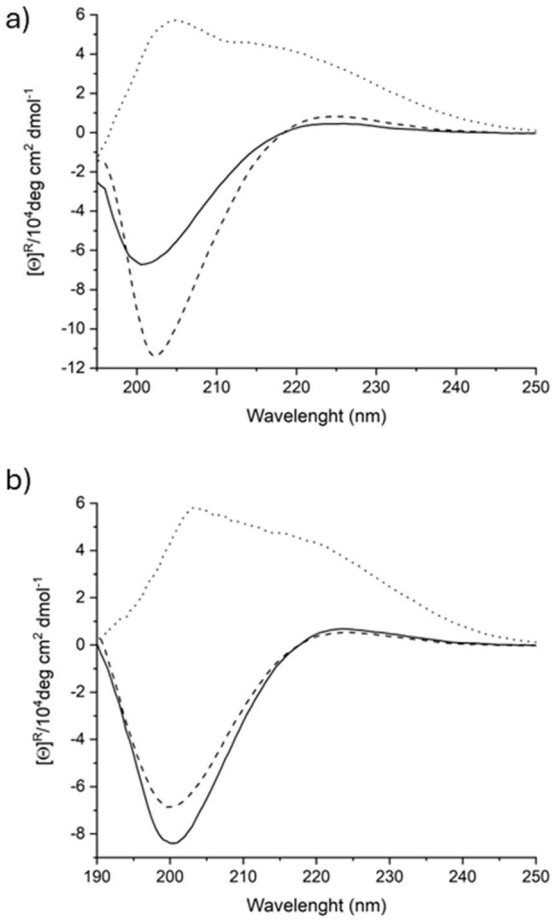

5. Figure ECD curves of 1 mM solutions of 1 (solid), 2 (dashed) and 3 (dotted) in methanol (a) and in water (b). Intensities were normalized for the number of chromophores (126)

The ECD spectrum of compound **1** in methanol exhibited a weak positive Cotton effect near 226 nm and a pronounced negative band at approximately 200 nm—features characteristic of a right-handed H12 helical conformation. In aqueous solution, the positive band persisted at 223 nm, while the negative band at 201 nm showed a marked increase in intensity. These observations suggest that the H12 helical structure is

preserved in water and may even exhibit enhanced stability, potentially due to solvent-induced self-association.

For compound **2**, the ECD spectrum in methanol revealed a positive band at 225 nm and a more intense negative band at 202 nm. These slight bathochromic shifts, relative to compound **1**, are indicative of a more compact helical structure, consistent with the formation of an H14 helix. In aqueous solution, the positive band appeared at 224 nm and the negative band shifted to 200 nm, albeit with reduced intensity. This solvent-dependent variation in spectral features supports the presence of an H14 helical fold and suggests that solvent polarity may influence the degree of helix stabilization and potential self-association.

In contrast, the ECD spectrum of compound **3** displayed a markedly different profile. Notably, the spectrum did not cross the baseline, a feature commonly associated with extended, strand-like conformations. In methanol, two positive bands were observed at 212 nm and 204 nm, and a similar pattern was retained in aqueous solution, with comparable intensities. These results indicate that the strand-like conformation of compound **3** is largely unaffected by solvent environment. The incorporation of the quaternary ammonium group via betaine conjugation significantly enhanced solubility in both methanol and water, thereby enabling reliable ECD measurements in both media.

4.1.2.3. FT-IR

To complement the structural characterization, Fourier-transform infrared (FT-IR) spectroscopy was employed to investigate the conformational features of compounds **1–3**.

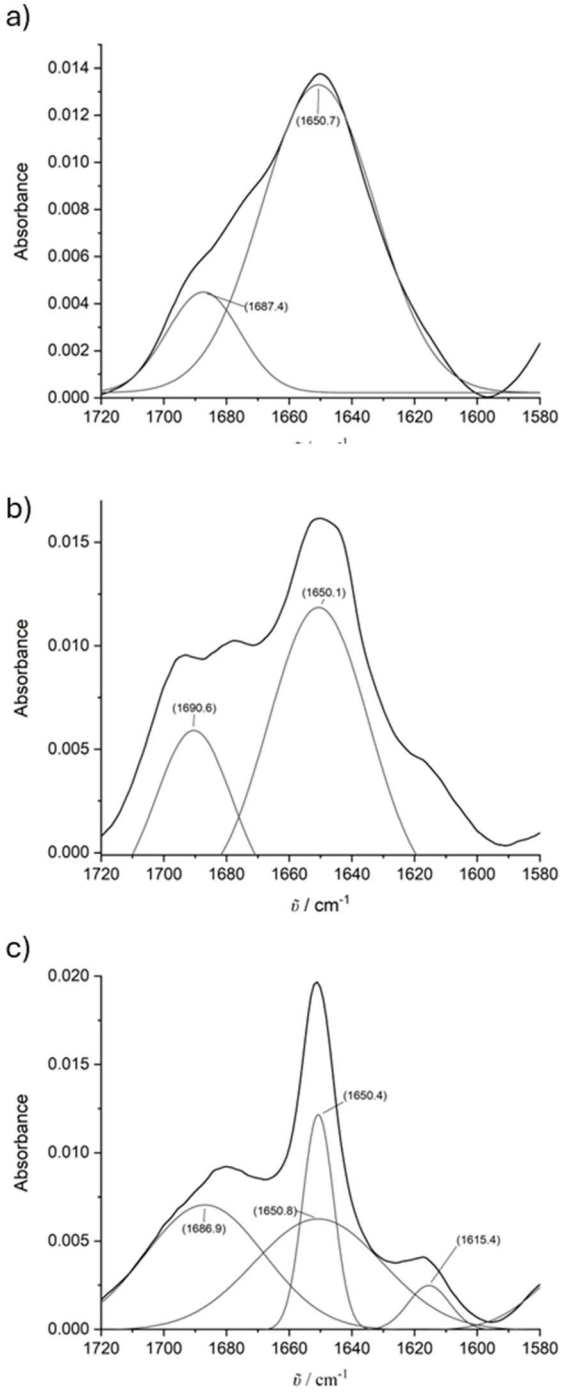

6. Figure FT-IR spectra in the amide I region of 1 (a), 2 (b) and 3 (c). Spectra were recorded for dry film samples from 1 mM peptide solution and normalized by the area. The solid and dash lines denote the measured and the fitted curves, respectively, whereas thin curves correspond to individual band components (using second derivative IR spectra and Fourier self deconvolution). (126)

The amide I region, primarily arising from the C=O stretching vibrations of the peptide backbone, provides insight into hydrogen bonding and secondary structure. For compound **1**, the deconvoluted amide I spectrum (*Figure 6*) exhibited a dominant band at

approximately 1641 cm^{-1}, indicative of strong intramolecular hydrogen bonding, consistent with a helical conformation. Additional shoulders at ~1685 cm^{-1} and ~1667 cm^{-1} likely correspond to weaker hydrogen bonds, such as those involving the C-terminal amide group. Although no reference FT-IR spectrum for the H12 helix is currently available, these spectral features strongly support the presence of a stable helical structure.

In the case of compound **2**, the deconvoluted amide I band revealed characteristic absorptions at ~1646, 1674, and 1690 cm^{-1}, corresponding to carbonyl groups engaged in varying degrees of hydrogen bonding. The relative intensities of the 1646 and 1690 cm^{-1} bands are consistent with the formation of an H14 helix. These findings corroborate the NMR data, suggesting that betaine conjugation promotes a shift from the expected H10 helix to an H14 helical fold.

Conversely, the FT-IR spectrum of compound **3** displayed a distinct pattern. A sharp band at ~1643 cm^{-1}, accompanied by a shoulder at ~1690 cm^{-1}, reflects the presence of both strong and weak hydrogen bonds. Additionally, a shoulder at ~1611 cm^{-1} suggests the involvement of intermolecular hydrogen bonding, characteristic of β-sheet-like, strand-based structures.

4.1.2.4. TEM

The markedly slow NH/ND exchange observed for compound **2**, along with the FT-IR data for compound **3**, implies the potential for self-association among the betaine-conjugated β-peptides. To further investigate this phenomenon, transmission electron microscopy (TEM) was conducted on aqueous solutions of the compounds at 4 mM concentration. Samples were imaged following dissolution and sonication (*Figure 7*).

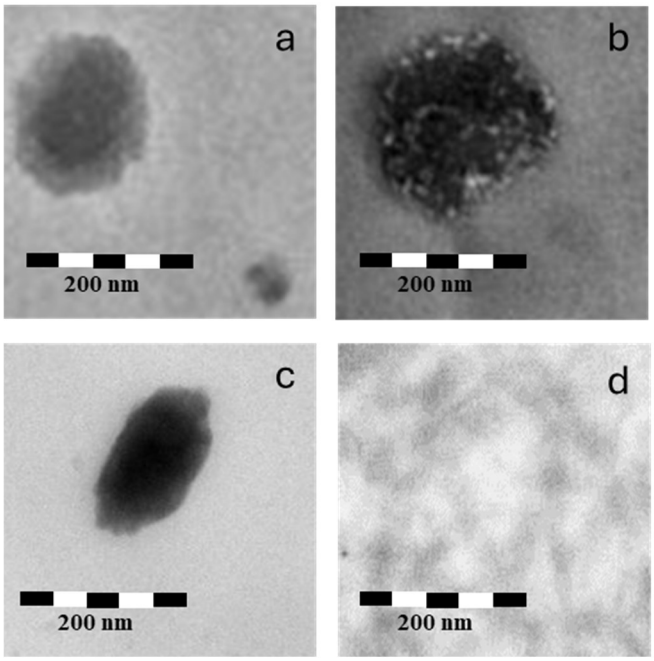

7. Figure TEM images of vesicles observed after dissolution and sonication of 4 mM solutions of 1 (a, b), 2 (c) and 3 (d) in water (126)

Remarkably, vesicle formation was observed for the helix-forming compounds **1** and **2** even in aqueous solution. This represents the first reported instance of a β-peptide adopting an H12 helical conformation that undergoes self-association into vesicular structures. Transmission electron microscopy (TEM) revealed vesicles with diameters ranging from approximately 130 to 200 nm for compound **1** (*Figure 7a and 7b*). For compound **2**, vesicles of slightly larger average diameter (~200 nm) were detected (*Figure 7c*).

The vesicles formed by compound **2** were assembled rapidly. Notably, vesicle formation occurred immediately upon dissolution and sonication, without the need for prolonged incubation. These findings suggest that the introduction of quaternary ammonium groups via betaine conjugation enhances the vertical amphiphilicity of β-peptides, thereby promoting self-association and vesicle formation. This highlights the dual role of betaine conjugation in modulating both secondary and higher-order (tertiary) structural organization. Importantly, the observation of vesicle formation in water—a biologically relevant solvent—underscores the potential applicability of these systems in aqueous environments.

In contrast, TEM analysis of compound **3** revealed a distinctly different morphology (*Figure 7d*). No vesicular structures were observed; instead, nanoscale fibrillar

assemblies were detected. This observation aligns with existing literature, which reports that peptides adopting strand-like conformations often exhibit a strong propensity for fibril formation. However, this study presents the first documented case of β-peptide fibril formation occurring in aqueous medium. Furthermore, the fibrils appeared to organize into an interconnected, net-like fibrinous architecture.

4.2. Peptide synthesis in a continuous-flow reactor

The development of CF-SPPS represents a significant advancement in the pursuit of sustainable chemical manufacturing. This methodology is particularly impactful within the framework of green chemistry, as it supports the reduction of hazardous reagent use and enhances overall process efficiency. Propylene carbonate (PC) is recognized as a green solvent due to its favorable environmental profile and sustainable production pathway. It is synthesized via the reaction of propylene oxide with carbon dioxide, a process that not only utilizes CO_2 — a major greenhouse gas — but also contributes to its reduction in the atmosphere. This transformation yields a solvent characterized by low toxicity, thereby enhancing safety for both human health and the environment.

Despite its numerous advantages, propylene carbonate (PC) has not yet seen widespread adoption in flow-based chemical synthesis. In this study, we aim to integrate PC into continuous-flow solid-phase peptide synthesis (CF-SPPS) protocols and develop a scalable CF-SPPS platform capable of producing peptides on a gram scale.

4.2.1. Determining the reaction conditions

A continuous-flow (CF) reactor system was employed in this study (*Figure 8*), comprising a high-performance liquid chromatography (HPLC) autosampler, an HPLC column thermostat equipped with a stainless-steel column, a semi-preparative HPLC pump, a back-pressure regulator, and a line selection valve system. This configuration enabled the recirculation of reagent solutions through the resin bed, facilitating efficient peptide synthesis.

The HPLC autosampler ensured precise and reproducible mixing and injection of reagents, while the semi-preparative HPLC pump provided pulse-free, consistent delivery of liquids. The peptide synthesis resin was packed into a stainless-steel column, which was thermally regulated using the HPLC column thermostat to maintain the desired reaction temperature. A back-pressure regulator was incorporated to stabilize system pressure, ensuring consistent flow conditions throughout the synthesis process.

Throughout the optimization process, the crude product purity was systematically monitored to evaluate the effectiveness of each set of conditions.

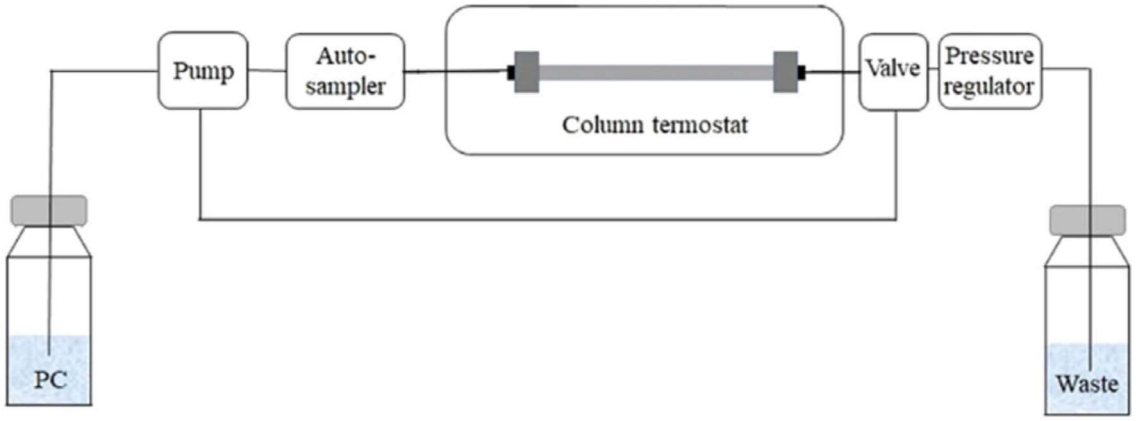

8. Figure Schematic illustration of the CF apparatus used. PC was used (127)

Initially, the temperature dependence of the coupling reaction was systematically investigated on 30, 50, 70 and 90 °C. The highest coupling efficiency was observed at 70 °C, indicating that elevated temperatures significantly enhance reaction kinetics.

After selecting the most optimal temperature, pressure was the next parameter to be investigated on 1, 20, 40, 60 and 80 bar. The results demonstrated that maintaining a moderate back-pressure was essential for ensuring consistent reagent flow and maximizing coupling performance. At 60 bar, the crude purity reached 96% and further increase in pressure did not improve the outcome. These findings underscore the importance of fine-tuning both thermal and pressure parameters to achieve optimal reaction conditions in CF-SPPS.

To enhance the efficiency of the synthesis process, the flow rate was systematically tested with 0.50, 0.30, 0.15 and 0.05 mL min^{-1}. The flow rate of 0.3 mL min^{-1} was found to maintain high crude product purity, demonstrating that increased throughput can be achieved without compromising the quality of the synthesized peptides.

The influence of amino acid equivalents on coupling efficiency was also systematically investigated with 1.5, 1.2, 1.0 and 0.8 equivalents. A reduction in the amount of amino acid resulted in significantly decreased crude product purity, indicating that a minimum threshold is required to maintain synthesis quality. The most optimal quantity is said to be 1.5 equivalents of amino acids.

In a further effort to minimize solvent consumption within the CF-system, the concentration of the coupling mixture was optimized. The investigated concentrations

were 300, 200, 100 and 50 mM. The excellent crude purity was preserved at a concentration of 100 mM, corresponding to the dissolution of 0.1 mmol of amino acid in 1 mL of PC. This result demonstrates that solvent usage can be substantially reduced without compromising the efficiency or outcome of the synthesis.

4.2.2. Synthesized α-peptides

The specified operational parameters were uniformly maintained throughout all synthetic procedures. Specifically, the thermostat was set to a constant temperature of 70 °C, the back-pressure regulator was adjusted to 60 bar, and the residence time was fixed at 5 minutes, corresponding to a flow rate of 0.3 mL min^{-1}. The column measuring 25 cm in length was packed with 300 mg of Tenta Gel R RAM resin. For the coupling reaction, 1.5 equivalents of amino acids were employed alongside 1.5 equivalents of the OxymaPure as the coupling agent, in the presence of 1.5 equivalents of *N,N*-diisopropylcarbodiimide (DIC). Reagent mixing was automated and conducted via the autosampler. Deprotection was achieved using a solution containing 2% piperidine and 2% 1,8-diazabicyclo[5.4.0]undec-7-ene (DBU) in PC. A washing step with PC was performed for 5 minutes between the coupling and deprotection stages.

To evaluate the performance of CF setup described above, an initial synthesis of a simple α-peptide (compound **4**) was conducted. Upon completion of the peptide chain assembly, the resin was removed from the column, and standard offline cleavage protocols were applied. The resulting crude peptide was lyophilized and subsequently analyzed using high-performance liquid chromatography coupled with mass spectrometry (HPLC-MS). As presented in *Table 1*, compound **4** was obtained with an isolated yield of 96% and a crude purity exceeding 98%, demonstrating the efficiency of the synthetic process.

1. Table Results of the synthesized α-peptides using PC as solvent at a 0.07 mmol scale (127)

Compound	Sequence of the peptide with one-letter code	Raw purity [%]	Yield [%]
4	ALFEK-NH_2	>98	96
5	KRLFKKLLFSLRKY-NH_2	>96	94
6	RQIKIWFQNRRMKWKK-NH_2	>97	93
7	GMASKAGAIAGKIAKVALKAL-NH_2	>95	91

Encouraged by these promising results, the CF setup was further applied to the synthesis of three additional α-peptide sequences (compounds **5**, **6**, and **7**), each possessing significant biomedical relevance. Specifically, compounds **5** and **7** correspond to the antimicrobial peptides DHVAR-4 and PGLA, respectively, while compound **6**, known as penetratin, is a well-characterized cell-penetrating peptide. The optimized CF-SPPS protocol proved to be both rapid and efficient, yielding high product purities and excellent isolated yields across all tested sequences. These findings underscore the robustness and effectiveness of the CF reaction setup, particularly when employing PC as the solvent medium.

4.2.3. Synthesized β-peptides

Given the satisfactory coupling efficiencies observed for longer peptide chains comprising up to 21 amino acids, the optimized CF synthesis protocol was further evaluated using more challenging sequences, specifically β-peptides. The incorporation of β-amino acids typically necessitates the use of specialized coupling reagents, such as 1-[bis(dimethylamino)methylene]-1*H*-1,2,3-triazolo[4,5-*b*]pyridinium 3-oxide hexafluorophosphate (HATU), in conjunction with *N,N*-diisopropylethylamine (DIPEA) as a base. However, upon mixing HATU and DIPEA in propylene carbonate (PC), minor precipitation was observed, which led to clogging of the reactor tubing.

To circumvent this issue, the previously validated coupling system — comprising OxymaPure and *N,N′*-diisopropylcarbodiimide (DIC) — was employed. Due to the inherently lower reactivity and steric hindrance associated with β-amino acids, the coupling reagents were recirculated through the resin bed by switching the valve system to recycling mode. Both coupling and deprotection steps were extended to 30 minutes to ensure completeness. The prolonged deprotection time was particularly important to the Fmoc removal in β-peptide compounds.

Using this modified protocol, β-peptides and a hybrid α/β-peptide (compound **1**, **2**, **3**, **8** and **9**) were successfully synthesized (*Figure 9*). Following chain assembly, the peptides were cleaved from the resin under standard conditions, lyophilized, and analyzed. The crude products exhibited excellent purities and good to excellent isolated yields. Further confirm the high purity of the crude peptides (*Table 2*) obtained after ethereal precipitation, thereby validating the robustness of the CF-SPPS method for the synthesis of structurally complex β- and α/β-peptides.

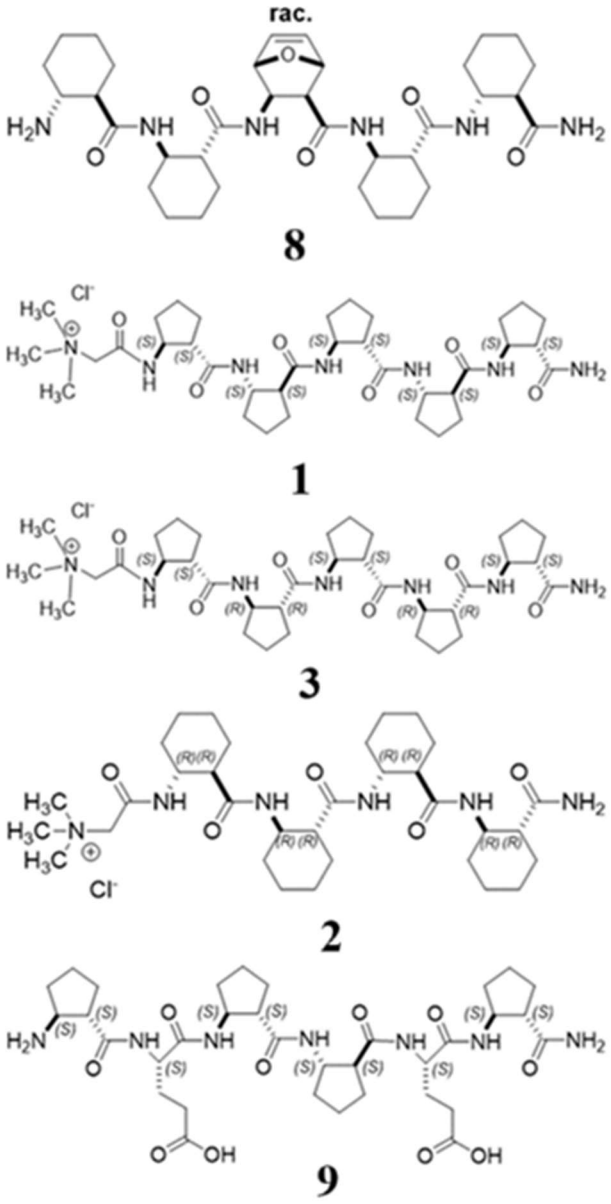

9. Figure Structures of the synthesized β-peptide foldamers using PC as solvent at a 0.07 mmol scale. (127)

2. Table Results of the synthesized β-peptide foldamers using PC as solvent at a 0.07 mmol scale. (127)

Entry	Compound	Raw purity [%]	Yield [%]
1	5	>96	89
2	6	>97	87
3	7	>98	86
4	8	>98	91
5	9	>98	93

4.2.4. Advantages of the upscaled peptide synthesis in a continuous-flow reaction

A direct comparison of the time required for peptide chain assembly under conventional SPPS conditions and the CF-SPPS protocol using PC as the solvent reveals a substantial difference in efficiency (*Table 3*). Both approaches were conducted at identical scales and with equivalent reagent concentrations to ensure comparability. For the manual SPPS process, coupling and deprotection durations were based on established literature protocols. The results clearly demonstrate that the CF-SPPS method significantly reduces synthesis time relative to traditional SPPS, highlighting the time-efficiency advantage of the CF approach.

3. Table Comparison of the time needed for the complete peptide chain assembly under the classic SPPS and the CF-SPPS conditions using PC as solvent at a 0.07 mmol scale. (127)

Compound	Classic SPPS [min][a)]	CF-SPPS [min][b)]
1	≈820	≈124
2	≈2260	≈334
3	≈2580	≈381
4	≈3380	≈498
5	≈1120	≈357
6 and 7	≈2560	≈427
8	≈2340	≈357
9	≈1100	≈240
[a)]Coupling time: 120 min, deprotection: 20 min, washing 20 min. [b)]Coupling time for 1–4 and for 5–9: 6.7 min and 30 min respectively, deprotection time for 1–4 and for 5–9: 6.7 and 30 min respectively, washing 10 min		

In addition to the accelerated reaction times, a notable benefit of the developed CF-SPPS methodology is its markedly reduced solvent consumption. As shown in *Table 4*, the volume of solvent required for CF-SPPS is minimal when compared to that used in conventional SPPS techniques. Quantitative analysis indicates that the CF-SPPS process utilizes approximately two orders of magnitude less solvent than traditional batch-based methods. This substantial reduction not only enhances the environmental sustainability

of the process but also contributes to lower operational costs, reinforcing the practical advantages of the CF-SPPS platform.

4. Table Comparison of the time needed for the complete peptide chain assembly under the classic SPPS and the CF-SPPS conditions using PC as solvent at a 0.07 mmol scale. (127)

Compound	Solvent used for peptide chain synthesis (mL)	
	Classic SPPS	CF-SPPS
1	~1680	~18.5
2	~4650	~50.1
3	~5310	~57.2
4	~6960	~74.7
5	~1680	~18.6
6 and **7**	~2010	~22.1
8	~1680	~18.6
9	~2010	~22.1

An additional objective of this study was to scale up the CF-SPPS process by employing HPLC columns with increased loading capacities. Building upon our previous findings and considering the geometrical parameters of larger columns, calculations were performed to determine the appropriate amount of resin required for complete and uniform packing, as well as the necessary flow rates to maintain a residence time of 5 minutes — both critical parameters for successful continuous-flow peptide synthesis.

For the scale-up experiments, two columns of identical length (250 mm) but differing internal diameters — 10 mm and 20 mm — were utilized. These configurations enabled synthesis at significantly larger scales, corresponding to 0.375 mmol and 1.5 mmol, respectively. For reference, previous work using a 4 mm diameter column of the same length demonstrated that 300 mg of resin was sufficient, with a flow rate of 0.3 mL min^{-1} ensuring a 5-minute residence time.

To adapt the process for larger columns, the internal volumes of the columns were first calculated. By subtracting the volume occupied by the packed resin from the total column volume, the dead volume—representing the solvent-filled space during synthesis—was determined. Dividing this dead volume by the target residence time yielded the required flow rate for each column configuration. The synthesis scale was then estimated by multiplying the mass of the packed resin by the loading capacity of the TentaGel R RAM resin (0.2 mmol g^{-1}).

5. Table Results of the synthesis of CF-SPPS carried out with a column with a diameter and length of 10 and 250 mm at a scale of 0.375 mmol. (127)

Compound	Isolated amount of peptide [mg]	Raw purity	Yield	Solvent used [mL]	Time needed [min]
2	794	>96%	84	≈626.8	≈334
3	993	>97%	87	≈714.6	≈381
4	782	>95%	86	≈933.9	≈498

To validate the accuracy of the scale-up calculations, three α-peptides (compound **2**, **3**, and **4**), each with significant biomedical relevance, were synthesized at a 0.375 mmol scale using a column with a 10 mm internal diameter. The outcomes of these syntheses are summarized in *Table 5*. In all cases, high crude purities and satisfactory isolated yields were achieved. Notably, peptide quantities approaching the gram scale were obtained within a total synthesis time of 5–8 hours for each sequence.

A key advantage of the process is the continued use of propylene carbonate (PC) as the reaction solvent. The total solvent consumption remained in the mL range, representing a reduction of approximately one order of magnitude compared to conventional SPPS protocols, which typically require solvent volumes in the liter range.

To further assess the robustness of the scale-up strategy, the synthesis of compound **3** (penetratin) was performed using a column with dimensions of 250 mm in length and 20 mm in diameter. The results are presented in *Table 6*.

6. Table Results of CF-SPPS synthesis carried out with a column possessing a diameter and length of 20 and 250 mm at a scale of 1.5 mmol (127)

Compound	Isolated amount of peptide [mg]	Raw purity	Yield	Solvent used [mL]	Time needed [min]
3	4154	>97%	91	≈2858.3	≈334

Remarkably, over 4 grams of penetratin were isolated in under 6 hours of synthesis time. Once again, PC was employed as the solvent, with total consumption remaining below 3 liters.

These findings underscore the efficiency, scalability, and sustainability of the developed continuous-flow platform for peptide synthesis.

5. Discussion

5.1. Betaine-conjugated foldamers

The conjugation of betaine significantly influenced the folding behavior, self-assembly properties, and solubility of a series of β-peptide foldamers. The oligomers were synthesized using an efficient continuous-flow solid-phase peptide synthesis (CF-SPPS) approach, which enabled the use of only a 1.5-fold excess of amino acids, highlighting the economic and scalable nature of the method.

For the homochiral [1*S*,2*S*]-ACPC pentamer (compound 1), betaine conjugation did not alter the characteristic H12 helical conformation. However, it markedly enhanced the oligomer's propensity for self-association, as evidenced by the formation of vesicles with diameters ranging from 130 to 180 nm in aqueous solution, as observed via transmission electron microscopy (TEM).

In the case of the [1*R*,2*R*]-ACHC tetramer (compound 2), betaine conjugation induced a notable shift in secondary structure, favoring the formation of an H14 helix over the expected H10 conformation. This structural transition was accompanied by a pronounced increase in self-association, with vesicles approximately 200 nm in diameter forming immediately upon dissolution and sonication.

For the alternating heterochiral [1*S*,2*S*]-ACPC/[1*R*,2*R*]-ACPC pentamer (compound 3), betaine conjugation primarily enhanced solubility in aqueous media. The expected extended strand (E-strand) conformation was retained, which facilitated self-assembly into amyloid-like fibrils. Interestingly, the presence of the betaine moiety subtly altered the aggregation behavior, resulting in the formation of a concatenated, fibrin-like network structure.

Overall, the observed self-association of all three betaine-conjugated β-peptide foldamers in aqueous environments underscores their potential for biomedical and materials science applications. These findings demonstrate that the introduction of alicyclic side chains and charged functional groups can be strategically employed to fine-tune both secondary and tertiary structural features of β-peptides.

The method was further validated through the successful synthesis of more structurally demanding sequences, including four β-peptide foldamers and an α/β-peptide chimera. For scale-up purposes, column geometries were optimized to accommodate increased resin loading and to maintain appropriate flow rates and residence times. This

optimization enabled peptide synthesis on a scale exceeding 4 grams, demonstrating the method's robustness and scalability.

A notable advantage of this approach is the minimal solvent requirement, which significantly enhances its environmental profile. The low solvent consumption, combined with high synthetic efficiency, aligns with the principles of green chemistry by reducing waste and improving overall sustainability. This advancement highlights the potential of CF-SPPS using PC as a solvent to meet the growing demand for greener and more efficient peptide synthesis technologies.

5.2. Upscaled synthesis

A rapid, environmentally sustainable, and highly efficient continuous-flow solid-phase peptide synthesis (CF-SPPS) platform has been developed for the synthesis of a broad range of peptides and foldamers using propylene carbonate (PC) as the solvent. The primary objective was to replace the commonly used dimethylformamide (DMF) with a more environmentally benign alternative. PC, identified as an optimal choice according to the GlaxoSmithKline (GSK) solvent selection guide, was selected for this purpose.

PC serves as a greener alternative to the traditionally used dimethylformamide (DMF). To assess its compatibility with CF-SPPS, four α-peptides were synthesized, yielding products of high purity and efficiency. To evaluate the compatibility of PC with CF-SPPS, four α-peptides were synthesized, all yielding high crude purities and demonstrating excellent synthetic efficiency. The robustness of the method was further validated through the successful synthesis of structurally complex sequences, including four β-peptide foldamers and an α/β-peptide chimera.

A key goal of this study was to scale up the methodology. Column geometries were carefully calculated to determine the appropriate resin loading and flow rates required to maintain optimal residence times. The scale-up was implemented in a stepwise manner, ultimately enabling peptide synthesis on a scale exceeding 4 grams with consistent efficiency.

A notable feature of this approach is the minimal use of PC, which significantly enhances the environmental profile of the process. The combination of low solvent consumption, high yield, and scalability aligns with the principles of green chemistry, offering a sustainable alternative for large-scale peptide production.

This advancement positions CF-SPPS using PC as a promising platform for greener peptide synthesis, with potential applications in pharmaceutical development and industrial-scale manufacturing.

6. Conclusions

The synthesized modified β-peptides fulfilled the intended concept and a well-defined structure was created, which is able to adopt a helical conformation in a self-assembling manner. The solubility of the β-amino acid peptide can be increased by the addition of betaines quaternary charge.

The structural modification of established β-peptide helices was achieved through N-terminal conjugation with betaine. This study investigated the three-dimensional self-organization of oligomers composed of [1*S*,2*S*]-2-aminocyclopentanecarboxylic acid (ACPC), [1*R*,2*R*]-2-aminocyclohexanecarboxylic acid (ACHC), and an alternating heterochiral homooligomer of [1*S*,2*S*]-ACPC and [1*R*,2*R*]-ACPC. Comprehensive structural analyses using NMR spectroscopy, electronic circular dichroism (ECD), FT-IR spectroscopy, and molecular modeling revealed that betaine conjugation did not alter the H12 helical conformation of the [1*S*,2*S*]-ACPC pentamer (compound 1). In contrast, the [1*R*,2*R*]-ACHC tetramer (compound 2) exhibited a significant conformational shift, adopting an H14 helix rather than the expected H10 structure.

Notably, this work presents the first evidence of self-association for a β-peptide adopting an H12 helical fold, with transmission electron microscopy (TEM) confirming vesicle formation. For the alternating heterochiral pentamer (compound 3), composed of [1*S*,2*S*]-ACPC and [1*R*,2*R*]-ACPC, betaine conjugation enhanced aqueous solubility and supported the formation of the anticipated extended strand (E-strand) conformation. TEM imaging revealed a fibrin-like network, indicative of strand-based self-assembly.

These findings demonstrate that betaine conjugation not only modulates solubility and secondary structure but also promotes higher-order assembly in aqueous environments. The introduction of quaternary ammonium groups offers new opportunities for the design of bioactive β-peptide foldamers with potential applications in receptor–ligand interactions and materials science.

In addition, the optimisation of a highly efficient, environmentally sustainable, and scalable continuous-flow solid-phase peptide synthesis (CF-SPPS) technology for the synthesis of various peptides and foldamers using propylene carbonate (PC) as the solvent. The primary objective was to replace dimethylformamide (DMF) with PC, an eco-friendly alternative recommended by the GSK solvent selection guide. To assess its compatibility with CF-SPPS, 4 distinct α-peptides were synthesized, yielding high purity

products. The efficacy of this method was further demonstrated through the successful synthesis of complex sequences, including four β-peptide foldamers and an α/β-peptide chimera.

An additional focus was the scalability of this approach. Geometric calculations were performed to determine the required resin quantity and optimal flow rate for achieving the desired residence time in larger columns. The scale-up process was conducted incrementally, demonstrating the capability of CF-SPPS to efficiently produce peptides at quantities exceeding 4 gramms. A notable advantage of this system is its use of PC as the solvent, which not only enhances sustainability but also minimizes solvent consumption. These attributes render the developed technology a promising advancement in peptide synthesis, with significant potential for broader applications in drug development and the pharmaceutical industry.

7. Summary

My PhD research encompassed multiple areas. Firstly, artificial self-assembling peptides were synthesized via solid-phase peptide synthesis, followed by N-terminal betaine conjugation to enhance their solubility. Structural characterization was performed using various techniques, including NMR, ECD, FT-IR, and TEM. These analyses confirmed that, in certain cases, structures capable of adopting helical conformations through self-organization were successfully formed. In other instances, betaine conjugation not only improved aqueous solubility but also promoted higher-order self-assembly in water, leading to the formation of complex supramolecular architectures. The introduction of quaternary ammonium groups offers new opportunities for the design of bioactive β-peptide foldamers with potential applications in receptor–ligand interactions and materials science.

Secondly, the optimization of automated peptide synthesis was focused on using a continuous-flow system. During the experimental work, the optimal reaction conditions such as optimal temperature, pressure, and flow rate were identified, while also minimizing the required amounts of reagents and solvents. The next task was aimed to scale up the continuous-flow solid-phase peptide synthesis (CF-SPPS) process by utilizing high-performance liquid chromatography (HPLC) columns with increased loading capacities. To adjust the synthesis process for larger columns, internal volumes were calculated, subtracting the resin-occupied space from the total column volume to determine the solvent-filled dead volume. Dividing this dead volume by the residence time provided the required flow rate for each column configuration. The synthesis scale was then estimated by multiplying the mass of the packed resin by the loading capacity of TentaGel R RAM resin (0.2 mmol g^{-1}). These methodological refinements contribute to the advancement of scalable and efficient peptide synthesis techniques. One of the major challenges was to render the synthesis process environmentally friendly; this was achieved through the use of PC as a solvent. This green solvent effectively replaced DMF without compromising peptide yield and purity.

8. References

1. Mitsueda A, Shimatani Y, Ito M, Ohgita T, Yamada A, Hama S, Graslund A, Lindberg S, Langel Ü, Harashima H, Nakase I, Futaki S, Kogure K, Development of a Novel Nanoparticle by Dual Modification With the Pluripotential Cell-penetrating Peptide PepFect6 for Cellular Uptake, Endosomal Escape, and Decondensation of an siRNA Core Complex. Biopolymers. 2013;100(6):698-704.
2. Lopez MJ, Mohiuddin SS. Biochemistry, Essential Amino Acids. StatPearls. Treasure Island (FL)2025.
3. Li J, Huang J, Ao Y, Li S, Yu M, Yu Z, Zhu L, Zhang Y, Yang X, Synergizing Upconversion Nanophotosensitizers With Hyperbaric Oxygen to Remodel the Extracellular Matrix for Enhanced Photodynamic Cancer Therapy. Acs Applied Materials & Interfaces. 2018;10(27):22985-96.
4. Veenstra VL, Damhofer H, Waasdorp C, Rijssen LBv, Marc JvdV, Dijk F, Wilmink H W, Besselink M G, Busch O R, Chang D K, Bailey P J, Biankin A V, Kocher H M, Medema J P, Li J S, Jiang R, Pierce D W, van Laarhoven H W M, Bijlsma M F, ADAM12 Is a Circulating Marker for Stromal Activation in Pancreatic Cancer and Predicts Response to Chemotherapy. Oncogenesis. 2018;7(11).
5. Mandity IM, Fulop F. An overview of peptide and peptoid foldamers in medicinal chemistry. Expert Opin Drug Discov. 2015;10(11):1163-77.
6. Wang C, Rao R, Cai Z, Yang H, Zhang L, Ji S, Zhang C, Gao D, Hu Y, Li J, Xiong W, Jiang H, Chu J, Wu D, Microclaw Array Fabricated by Single Exposure of Femtosecond Airy Beam and Self-Assembly for Regulating Cell Migratory Plasticity. Acs Nano. 2023;17(10):9025-38.
7. Zhao Y, Jiang H, Yu J, Wang L, Du J. Engineered Histidine-Rich Peptides Enhance Endosomal Escape for Antibody-Targeted Intracellular Delivery of Functional Proteins. Angewandte Chemie. 2023;135(38).
8. Simon RJ, Kania RS, Zuckermann RN, Huebner VD, Jewell DA, Banville S, NG S, Wang L, Rosenberg S, Marlowe C K, Peptoids: a modular approach to drug discovery. Proc Natl Acad Sci U S A. 1992;89(20):9367-71.
9. Henke E, Nandigama R, Ergün S. Extracellular Matrix in the Tumor Microenvironment and Its Impact on Cancer Therapy. Frontiers in Molecular Biosciences. 2020;6.
10. Lu Y, Chen Y, Hou G, Lei H, Liu L, Huang X, Sun S, Liu L, Liu X, Na J, Zhao Y, Cheng L, Zhong L, Zinc–Iron Bimetallic Peroxides Modulate the Tumor Stromal Microenvironment and Enhance Cell Immunogenicity for Enhanced Breast Cancer Immunotherapy Therapy. Acs Nano. 2024;18(15):10542-56.
11. Ji T, Lang J, Wang J, Cai R, Zhang Y, Qi F, Zhang L, Zhao X, Wu W, Hao J, Qin Z, Zhao Y, Nie G, Designing Liposomes to Suppress Extracellular Matrix Expression to Enhance Drug Penetration and Pancreatic Tumor Therapy. Acs Nano. 2017;11(9):8668-78.
12. Ding M, Zhang Y, Li J, Pu K. Bioenzyme-Based Nanomedicines for Enhanced Cancer Therapy. Nano Convergence. 2022;9(1).
13. Wang Y, Chu Y, Ren X, Xiang H, Xi Y, Ma X, Zhu K, Guo Z, Zhou C, Zhang G, Chen B, Epidural Adipose Tissue-Derived Mesenchymal Stem Cell Activation Induced by Lung Cancer Cells Promotes Malignancy and EMT of Lung Cancer. Stem Cell Research & Therapy. 2019;10(1).

14. Gong H, Chao Y, Xiang J, Han X, Song G, Feng L, Liu J, Yang G, Chen Q, Liu Z, Hyaluronidase to Enhance Nanoparticle-Based Photodynamic Tumor Therapy. Nano Letters. 2016;16(4):2512-21.
15. Mirloup A, Berthomé Y, Riché S, Wagner P, Hanser F, Laurent A, Iturrioz X, Llorens-Cortes C, Karpenko J, Bonnet D, Alared: Solvatochromic and Fluorogenic Red Amino Acid for Ratiometric Live-Cell Imaging of Bioactive Peptides. Chemistry - A European Journal. 2024;30(35).
16. Mirloup A, Berthomé Y, Riché S, Wagner P, Hanser F, Laurent A, Iturrioz X, Llorens-Cortes C, Karpenko J, Bonnet D, Alared: Environmentally Sensitive Fluorescent Red Amino Acid for Biomolecular Interaction Studies and Live-Cell Imaging of Bioactive Peptides. 2023.
17. Yang D, Kim BJ, He H, Xu B. Enzymatically Forming Cell Compatible Supramolecular Assemblies of Tryptophan-rich Short Peptides. Peptide Science. 2020;113(2).
18. Yang J, Li Q, Yang X, Feng Y, Ren X, Shi C, Zhang W, Multitargeting Gene Delivery Systems for Enhancing the Transfection of Endothelial Cells. Macromolecular Rapid Communications. 2016;37(23):1926-31.
19. Abyaneh HS, Regenold M, McKee TD, Allen C, Gauthier MA. Towards Extracellular Matrix Normalization for Improved Treatment of Solid Tumors. Theranostics. 2020;10(4):1960-80.
20. Wang T, Yang S, Petrenko VA, Torchilin VP. Cytoplasmic Delivery of Liposomes Into McF-7 Breast Cancer Cells Mediated by Cell-Specific Phage Fusion Coat Protein. Molecular Pharmaceutics. 2010;7(4):1149-58.
21. Bock N, Forouz F, Hipwood L, Clegg J, Jeffery PL, Gough M, van Wyngaard T, Pyke C, Adams M N, Bray L J, Croft L, Thompson E W, Kryza T, Meinert C, GelMA, Click-Chemistry Gelatin and Bioprinted Polyethylene Glycol-Based Hydrogels as 3D Ex Vivo Drug Testing Platforms for Patient-Derived Breast Cancer Organoids. Pharmaceutics. 2023;15(1):261.
22. Seebach D, Gardiner J. Beta-peptidic peptidomimetics. Acc Chem Res. 2008;41(10):1366-75.
23. Allison JR, Muller M, van Gunsteren WF. A comparison of the different helices adopted by alpha- and beta-peptides suggests different reasons for their stability. Protein Sci. 2010;19(11):2186-95.
24. Bellesia G, Shea JE. Structure and stability of amyloid fibrils formed from synthetic beta-peptides. Front Biosci. 2008;13:6957-65.
25. Ahmed S, Kaur K. The proteolytic stability and cytotoxicity studies of L-aspartic acid and L-diaminopropionic acid derived beta-peptides and a mixed alpha/beta-peptide. Chem Biol Drug Des. 2009;73(5):545-52.
26. Mangelschots J, Bibian M, Gardiner J, Waddington L, Van Wanseele Y, Van Eeckhaut A, Acevedo M M D, Mele B V, Madder A, Hoogenboom R, Ballet S, Mixed alpha/beta-Peptides as a Class of Short Amphipathic Peptide Hydrogelators with Enhanced Proteolytic Stability. Biomacromolecules. 2016;17(2):437-45.
27. Miller CA, Gellman SH, Abbott NL, de Pablo JJ. Mechanical stability of helical beta-peptides and a comparison of explicit and implicit solvent models. Biophys J. 2008;95(7):3123-36.
28. Hook DF, Bindschadler P, Mahajan YR, Sebesta R, Kast P, Seebach D. The proteolytic stability of 'designed' beta-peptides containing alpha-peptide-bond mimics

and of mixed alpha,beta-peptides: application to the construction of MHC-binding peptides. Chem Biodivers. 2005;2(5):591-632.
29. Miller JP, Melicher MS, Schepartz A. Positive allostery in metal ion binding by a cooperatively folded beta-peptide bundle. J Am Chem Soc. 2014;136(42):14726-9.
30. Daura X, Gademann K, Schafer H, Jaun B, Seebach D, van Gunsteren WF. The beta-peptide hairpin in solution: conformational study of a beta-hexapeptide in methanol by NMR spectroscopy and MD simulation. J Am Chem Soc. 2001;123(10):2393-404.
31. Dong N, Chou S, Li J, Xue C, Li X, Cheng B, Shan A, Xu L, Short Symmetric-End Antimicrobial Peptides Centered on beta-Turn Amino Acids Unit Improve Selectivity and Stability. Front Microbiol. 2018;9:2832.
32. Quiros A, del Mar Contreras M, Ramos M, Amigo L, Recio I. Stability to gastrointestinal enzymes and structure-activity relationship of beta-casein-peptides with antihypertensive properties. Peptides. 2009;30(10):1848-53.
33. Gopalan RD, Del Borgo MP, Mechler AI, Perlmutter P, Aguilar MI. Geometrically Precise Building Blocks: the Self-Assembly of beta-Peptides. Chem Biol. 2015;22(11):1417-23.
34. Imamura Y, Umezawa N, Osawa S, Shimada N, Higo T, Yokoshima, Fukuyama T, Iwatsubo T, Kato N, Tomita T, Higuchi T, Effect of Helical Conformation and Side Chain Structure on Γ-Secretase Inhibition by B-Peptide Foldamers: Insight Into Substrate Recognition. Journal of Medicinal Chemistry. 2013;56(4):1443-54.
35. Martinek TA, Fulop F. Side-chain control of beta-peptide secondary structures. Eur J Biochem. 2003;270(18):3657-66.
36. Appella DH, Christianson LA, Klein DA, Powell DR, Huang X, Barchi JJ, Jr., Gellman S Residue-based control of helix shape in beta-peptide oligomers. Nature. 1997;387(6631):381-4.
37. Cussol L, Mauran-Ambrosino L, Buratto J, Belorusova AY, Neuville M, Ősz J, Fribourg S, Fremaux J, Dolain C, Goudreau S R, Rochel N, Guichard G, Structural Basis for A-Helix Mimicry and Inhibition of Protein–Protein Interactions With Oligourea Foldamers. Angewandte Chemie. 2020;133(5):2326-33.
38. Dengler S, Mandal PK, Allmendinger L, Douat C, Huc I. Conformational Interplay in Hybrid Peptide–helical Aromatic Foldamer Macrocycles. Chemical Science. 2021;12(33):11004-12.
39. Wang PS, Schepartz A. beta-Peptide bundles: Design. Build. Analyze. Biosynthesize. Chem Commun (Camb). 2016;52(47):7420-32.
40. Watanabe M, Nagata M, Doi R, Uemura M, Ochiai N, Ichinose W, Fujiwara K, Sato Y, Kameda T, Takeuchi K, Shuto S, Helix-Forming Aliphatic Homo-Δ-Peptides Foldamers Based on Conformational Restriction of Cyclopropane. 2022.
41. Dalafave DS, Prisco G. Inhibition of Antiapoptotic BCL-XL, BCL-2, and McL-1 Proteins by Small Molecule Mimetics. Cancer Informatics. 2010;9:CIN.S5065.
42. Kulkarni K, Habila N, Del Borgo MP, Aguilar MI. Novel Materials From the Supramolecular Self-Assembly of Short Helical beta(3)-Peptide Foldamers. Front Chem. 2019;7:70.
43. Bouillere F, Thetiot-Laurent S, Kouklovsky C, Alezra V. Foldamers containing gamma-amino acid residues or their analogues: structural features and applications. Amino Acids. 2011;41(3):687-707.
44. Just D, Palivec V, Bártová K, Bednářová L, Pazderková M, Císařová I, Martinez-Seara H, Jahn U, Foldamers Controlled by Functional Triamino Acids:

Structural Investigation of A/Γ-Hybrid Oligopeptides. Communications Chemistry. 2024;7(1).
45. Takechi-Haraya Y, Ohgita T, Kotani M, Kono H, Saito C, Tamagaki-Asahina H, Nishitsuji K, Uchimura K, Sato T, Kawano R, Sakai-Kato K, Izutsu K, Saito H, Effect of Hydrophobic Moment on Membrane Interaction and Cell Penetration of Apolipoprotein E-Derived Arginine-Rich Amphipathic A-Helical Peptides. Scientific Reports. 2022;12(1).
46. Dongrui Z, Miyamoto M, Yokoo H, Demizu Y. Innovative peptide architectures: advancements in foldamers and stapled peptides for drug discovery. Expert Opin Drug Discov. 2024;19(6):699-723.
47. Dangi A, Pande BM, Agrawal S, Sarkar D, Vamkudoth KR, Marelli UK. Total Synthesis, Structure Elucidation and Expanded Bioactivity of Icosalide A: Effect of Lipophilicity and Ester to Amide Substitution on Its Bioactivity. Organic & Biomolecular Chemistry. 2023;21(28):5725-31.
48. Sang P, Cai J. Unnatural helical peptidic foldamers as protein segment mimics. Chem Soc Rev. 2023;52(15):4843-77.
49. Hamley IW. Biocatalysts Based on Peptide and Peptide Conjugate Nanostructures. Biomacromolecules. 2021;22(5):1835-55.
50. Tallet L, Frisch E, Bornerie M, Medemblik C, Frisch B, Lavalle P, Guichard G, Douat C, Kichler A, Design of Oligourea-Based Foldamers with Antibacterial and Antifungal Activities. Molecules. 2022;27(5).
51. Eccles N, Della Sala F, Le Bailly BAF, Whitehead GFS, Clayden J, Webb SJ. Molecular Recognition by Zn(II)-Capped Dynamic Foldamers. ChemistryOpen. 2020;9(3):338-45.
52. Aguilar MI, Purcell AW, Devi R, Lew R, Rossjohn J, Smith AI, Perlmutter P, Beta-amino acid-containing hybrid peptides--new opportunities in peptidomimetics. Org Biomol Chem. 2007;5(18):2884-90.
53. Ghosh N, Kundu LM. In-situ side-chain peptide cyclization as a breaker strategy against the amyloid aggregating peptide. Bioorg Med Chem. 2021;33:116017.
54. Tran TT, McKie J, Meutermans WD, Bourne GT, Andrews PR, Smythe ML. Topological side-chain classification of beta-turns: ideal motifs for peptidomimetic development. J Comput Aided Mol Des. 2005;19(8):551-66.
55. Heath SL, Horne WS, Lengyel GA. Effects of chirality and side chain length in C(alpha,alpha)-dialkylated residues on beta-hairpin peptide folded structure and stability. Org Biomol Chem. 2023;21(31):6320-4.
56. Liu R, Dong X, Seroski DT, Soto Morales B, Wong KM, Robang AS, Melgar L, Angelini T E, Paravastu A K, Hall C K, Hudalla G A, Side-Chain Chemistry Governs Hierarchical Order of Charge-Complementary beta-sheet Peptide Coassemblies. Angew Chem Int Ed Engl. 2023;62(51):e202314531.
57. Cheng RP, Gellman SH, DeGrado WF. beta-Peptides: from structure to function. Chem Rev. 2001;101(10):3219-32.
58. Gorrea E, Pohl G, Nolis P, Celis S, Burusco KK, Branchadell V, Perczel A, Ortuno R M, Secondary Structure of Short B-Peptides as the Chiral Expression of Monomeric Building Units: A Rational and Predictive Model. The Journal of Organic Chemistry. 2012;77(21):9795-806.
59. Sinatra L, Kolano L, Icker M, Fritzsche SR, Volke D, Gockel I, Thieme R, Hoffmann R, Hansen F K, Hybrid Peptides Based on A-Aminoxy Acids as Antimicrobial and Anticancer Foldamers. Chempluschem. 2021;86(6):827-35.

60. Zhang Y, Fang Z, Pan D, Li Y, Zhou J, Chen H, Su L, Wu Y, Ding H, Shen X, Gong Q, Luo K, Dendritic Polymer-Based Nanomedicines Remodel the Tumor Stroma: Improve Drug Penetration and Enhance Antitumor Immune Response. Advanced Materials. 2024;36(25).
61. Chongsiriwatana NP, Patch JA, Czyzewski AM, Dohm MT, Ivankin A, Gidalevitz D, Zuckermann R N, Barron A E, Peptoids that mimic the structure, function, and mechanism of helical antimicrobial peptides. Proc Natl Acad Sci U S A. 2008;105(8):2794-9.
62. Stephens OM, Kim S, Welch BD, Hodsdon ME, Kay MS, Schepartz A. Inhibiting HIV fusion with a beta-peptide foldamer. J Am Chem Soc. 2005;127(38):13126-7.
63. Gkogka I, Glykos NM. Folding molecular dynamics simulation of T-peptide, a HIV viral entry inhibitor: Structure, dynamics, and comparison with the experimental data. J Comput Chem. 2022;43(14):942-52.
64. Gopalakrishnan R, Frolov AI, Knerr L, Drury WJ, 3rd, Valeur E. Therapeutic Potential of Foldamers: From Chemical Biology Tools To Drug Candidates? J Med Chem. 2016;59(21):9599-621.
65. Klein M. Stabilized helical peptides: overview of the technologies and its impact on drug discovery. Expert Opin Drug Discov. 2017;12(11):1117-25.
66. Oba M. Cell-Penetrating Peptide Foldamers: Drug-Delivery Tools. Chembiochem. 2019;20(16):2041-5.
67. Das TN, Ramesh A, Ghosh A, Moyra S, Maji TK, Ghosh G. Peptide-based nanomaterials and their diverse applications. Nanoscale Horiz. 2025;10(2):279-313.
68. Lyubchenko YL. Protein Self-Assembly at the Liquid-Surface Interface. Surface-Mediated Aggregation Catalysis. J Phys Chem B. 2023;127(9):1880-9.
69. Hamley IW. Self-Assembly, Bioactivity, and Nanomaterials Applications of Peptide Conjugates with Bulky Aromatic Terminal Groups. ACS Appl Bio Mater. 2023;6(2):384-409.
70. Gunasekara RW, Zhao Y. Conformationally switchable water-soluble fluorescent bischolate foldamers as membrane-curvature sensors. Langmuir. 2015;31(13):3919-25.
71. Beharry AA, Sadovski O, Woolley GA. Photo-control of peptide conformation on a timescale of seconds with a conformationally constrained, blue-absorbing, photo-switchable linker. Org Biomol Chem. 2008;6(23):4323-32.
72. Giuliani A, Rinaldi AC. Beyond natural antimicrobial peptides: multimeric peptides and other peptidomimetic approaches. Cell Mol Life Sci. 2011;68(13):2255-66.
73. Wang MD, Yi L, Li Y, Xu R, Hu J, Hou DY, Liu C, Wang H, Homologous Peptide Foldamer Promotes FUS Aggregation and Triggers Cancer Cell Death. J Am Chem Soc. 2024;146(42):28669-76.
74. Vezenkov LL, Martin V, Bettache N, Simon M, Messerschmitt A, Legrand B, Bantignies J, Subra G, Maynadier M, Bellet V, Garcia M, Martinez J, Amblard M, Ribbon-like Foldamers for Cellular Uptake and Drug Delivery. Chembiochem. 2017;18(21):2110-4.
75. De Giorgi M, Voisin-Chiret AS, Rault S. Targeting the BH3 domain of Bcl-2 family proteins. A brief history from natural products to foldamers as promising cancer therapeutic avenues. Curr Med Chem. 2013;20(24):2964-78.

76. Ahmed J, Fitch TC, Donnelly CM, Joseph JA, Ball TD, Bassil MM, Son A, Zhang C, Ledreux A, Horowitz S, Qin Y, Paredes D, Kumar S, Foldamers reveal and validate therapeutic targets associated with toxic alpha-synuclein self-assembly. Nat Commun. 2022;13(1):2273.
77. Tilly D, Cullen W, Zhong H, Jamagne R, Vitórica-Yrezábal ÍJ, Webb SJ. A-Amino-<i>iso</I>-Butyric Acid Foldamers Terminated With Rhodium(I) N-Heterocyclic Carbene Catalysts. Chemistry - A European Journal. 2022;28(9).
78. Lister FGA, Eccles N, Pike SJ, Brown RA, Whitehead GFS, Raftery J, Webb S J, Clayden J, Bis-Pyrene Probes of Foldamer Conformation in Solution and in Phospholipid Bilayers. Chemical Science. 2018;9(33):6860-70.
79. Fülöp L, Mándity IM, Juhász G, Szegedi V, Hetényi A, Wéber E, Bozsó Zs, Simon D, Benkő M, Király Z, Martinek T A, A Foldamer-Dendrimer Conjugate Neutralizes Synaptotoxic B-Amyloid Oligomers. Plos One. 2012;7(7):e39485.
80. Li W, Jiang M, Liu M, Xu L, Xia YQ, Wan L, Chen F, Development of a Fully Continuous-Flow Approach Towards Asymmetric Total Synthesis of Tetrahydroprotoberberine Natural Alkaloids. Chemistry - A European Journal. 2022;28(33).
81. McCaw PG, Deadman BJ, Maguire AR, Collins SG. Delivering Enhanced Efficiency in the Synthesis of A-Diazosulfoxides by Exploiting the Process Control Enabled in Flow. Journal of Flow Chemistry. 2016;6(3):226-33.
82. Jiang M, Liu M, Huang HS, Chen FE. Fully Continuous Flow Synthesis of 5-(Aminomethyl)-2-Methylpyrimidin-4-Amine: A Key Intermediate of Vitamin B₁. Organic Process Research & Development. 2021;25(10):2331-7.
83. Nqeketo S, Watts P. Synthesis of Dolutegravir Exploiting Continuous Flow Chemistry. The Journal of Organic Chemistry. 2023;88(16):12024-40.
84. Liu Z, Wakihara T, Nomura N, Matsuo T, Anand C, Elangovan SP, Yanaba Y, Yoshikawa T, Okubo T, Ultrafast and Continuous Flow Synthesis of Silicoaluminophosphates. Chemistry of Materials. 2016;28(13):4840-7.
85. Noël T, Buchwald SL. Cross-Coupling in Flow. Chemical Society Reviews. 2011;40(10):5010.
86. Feng K, Zhu Y, Gu SX, Jiao L, Wang H. Typical Cases of Continuous Flow Chemistry in Pharmaceutical Synthesis in 2023–2024. Asian Journal of Organic Chemistry. 2025;14(5).
87. Zhang S, Junkers T, Kuhn S. Continuous-flow self-supported seATRP using a sonicated microreactor. Chem Sci. 2022;13(42):12326-31.
88. Wu H, Du X, Meng X, Qiu D, Qiao Y. A three-tiered colloidosomal microreactor for continuous flow catalysis. Nat Commun. 2021;12(1):6113.
89. Yu Z, Tong G, Xie X, Zhou P, Lv Y, Su W. Continuous-Flow Process for the Synthesis of 2-Ethylphenylhydrazine Hydrochloride. Organic Process Research & Development. 2015;19(7):892-6.
90. Fanelli F, Parisi G, Degennaro L, Luisi R. Contribution of microreactor technology and flow chemistry to the development of green and sustainable synthesis. Beilstein J Org Chem. 2017;13:520-42.
91. Sagandira CR, Akwi FM, Sagandira MB, Watts P. Multistep Continuous Flow Synthesis of Stavudine. The Journal of Organic Chemistry. 2021;86(20):13934-42.
92. Jiao J, Nie W, Yu T, Yang F, Zhang Q, Aihemaiti F, Yang T, Liu X, Wang J, Li P, Multi-Step Continuous-Flow Organic Synthesis: Opportunities and Challenges. Chemistry. 2021;27(15):4817-38.

93. Cambié D, Bottecchia C, Straathof NJW, Hessel V, Noël T. Applications of Continuous-Flow Photochemistry in Organic Synthesis, Material Science, and Water Treatment. Chemical Reviews. 2016;116(17):10276-341.
94. Yu Z, Lv Y, Yu C. A Continuous Kilogram-Scale Process for the Manufacture of <i>o</I>-Difluorobenzene. Organic Process Research & Development. 2012;16(10):1669-72.
95. Britton J, Raston CL. Multi-step continuous-flow synthesis. Chem Soc Rev. 2017;46(5):1250-71.
96. Sun M, Yang J, Fu Y, Liang C, Li H, Yan G, Yin C, Yu W, Ma Y, Cheng R, Ye J, Continuous Flow Process for the Synthesis of Betahistine via Aza-Michael-Type Reaction in Water. Organic Process Research & Development. 2021;25(5):1160-6.
97. Zhou J, Zhang W, Bai S, Shao Y-H, Tang Y, Jing MH, Yu Z, Kinetics Research and Process Development for the Intensification of the Fully Continuous Flow Synthesis of 3-Amino-1-Adamantanol. Chemical Engineering & Technology. 2025;48(5).
98. Ma X, Jin-sha C, Du X. A Continuous Flow Process for the Synthesis of Hymexazol. Organic Process Research & Development. 2019;23(6):1152-8.
99. Zhang A, Xu J, Li Y, Hu M, Lin Z, Song Y, Qi J, Chen W, Liu Z, Cheng Y, Three-Dimensional Large-Scale Fused Silica Microfluidic Chips Enabled by Hybrid Laser Microfabrication for Continuous-Flow UV Photochemical Synthesis. Micromachines. 2022;13(4):543.
100. Cao L, Kim HW, Jeong YJ, Han SC, Park JK. Rapid Continuous-Flow Water-Free Synthesis of Ultrapure Ionic Liquids Assisted by Microwaves. Organic Process Research & Development. 2022;26(1):207-14.
101. Hosoya M, Manaka A, Kawajiri T, Ohara T. Application of Taylor Vortex Flow Reactor Enabling Precise Control of Nucleation in Reactive Crystallization. 2023.
102. Fong EJ, Han J, Cornell CC, Han Y. Opportunities and Challenges for Nanoparticle Synthesis Using Continuous Flow Systems: A Magnetite Nanocluster Case Study. 2019.
103. Thankappan H, Burke CM, Glennon B. Indium Chloride Catalysed Benzyl Bromination Using Continuous Flow Technology. Organic & Biomolecular Chemistry. 2023;21(3):508-13.
104. Dong K, Sun C, Song J, Wei GX, Pang SP. Synthesis of 2,6,8,12-Tetraacetyl-2,4,6,8,10,12-Hexaazaisowurtzitane (TAIW) From 2,6,8,12-Tetraacetyl-4,10-Dibenzyl-2,4,6,8,10,12-Hexaazaisowurtzitane (TADBIW) by Catalytic Hydrogenolysis Using a Continuous Flow Process. Organic Process Research & Development. 2014;18(11):1321-5.
105. Merrifield RB. Solid-phase peptide synthesis. Adv Enzymol Relat Areas Mol Biol. 1969;32:221-96.
106. Merrifield RB. Solid Phase Peptide Synthesis. I. The Synthesis of a Tetrapeptide. - Journal of the American Chemical Society. 1963; 85, (14), 2149–2154.
107. Mourtas S, Katakalou C, Gatos D, Barlos K. Convergent Synthesis of Thioether Containing Peptides. Molecules. 2020;25(1):218.
108. Li Y, Qu Q, Qi YK, Liu L, Wang K-W, Liu Y, Fang G, Comparison of Different Strategies Towards the Chemical Synthesis of Long-chain Scorpion Toxin AaH-II. Journal of Peptide Science. 2021;28(2).
109. Duo X, Bai L, Wang J, Ji H, Guo J, Ren X, Shi C, Xia S, Zhang W, Feng Y, CAGW and TAT-NLS Peptides Functionalized Multitargeting Gene Delivery System

With High Transfection Efficiency. Polymers for Advanced Technologies. 2019;30(10):2567-76.
110. Brodrecht M, Breitzke H, Gutmann T, Buntkowsky G. Biofunctionalization of Nano Channels by Direct In-Pore Solid-Phase Peptide Synthesis. Chemistry - A European Journal. 2018;24(67):17814-22.
111. Peterson CM, Helterbrand MR, Hartgerink JD. Covalent Capture of a Collagen Mimetic Peptide With an Integrin-Binding Motif. Biomacromolecules. 2022;23(6):2396-403.
112. Nasufović V, Küllmer F, Bößneck J, Dahse HM, Görls H, Bellstedt P, Stallforth P, Arndt H, Total Synthesis and Bioactivity Mapping of Geodiamolide H. Chemistry - A European Journal. 2021;27(45):11633-42.
113. Kallmyer NE, Rider NE, Reuel NF. Design and Validation of a Frugal, Automated, Solid-Phase Peptide Synthesizer. Plos One. 2020;15(8):e0237473.
114. Sharma A, Kumar A, de la Torre BG, Albericio F. Liquid-Phase Peptide Synthesis (LPPS): A Third Wave for the Preparation of Peptides. Chem Rev. 2022;122(16):13516-46.
115. Matsumoto T, Kuranaga T, Taniguchi Y, Wang W, Kakeya H. Solid-Phase Total Synthesis and Structural Confirmation of Antimicrobial Longicatenamide A. Beilstein Journal of Organic Chemistry. 2022;18:1560-6.
116. Sitnikov NS, Malysheva YB, Fedorov AY, Schmalz HG. Design and Synthesis of New Protease-Triggered CO-Releasing Peptide–Metal-Complex Conjugates. European Journal of Organic Chemistry. 2019;2019(40):6830-7.
117. Vivenzio G, Scala MC, Marino P, Manfra M, Campiglia P, Sala M. Dipropyleneglycol Dimethylether, New Green Solvent for Solid-Phase Peptide Synthesis: Further Challenges to Improve Sustainability in the Development of Therapeutic Peptides. Pharmaceutics. 2023;15(6):1773.
118. Casanova J, Villaraza AJL, Salvador-Reyes LA. Synthesis and Biological Evaluation of Cyanobacterial-Inspired Peptides. Scienggj. 2024;17(Supplement):42-88.
119. Mosbah A, Chouchane H, Abdelwahed S, Redissi A, Hamdi M, Kouidhi S, Neifar M, Masmoudi A S, Cherif A, Mnif W, Peptides Fixing Industrial Textile Dyes: A New Biochemical Method in Wastewater Treatment. Journal of Chemistry. 2019;2019:1-7.
120. Ramesh S, de la Torre BG, Albericio F, Kruger HG, Govender T. Microwave-Assisted Synthesis of Antimicrobial Peptides. Methods Mol Biol. 2017;1548:51-9.
121. Sosnowska M, Łęga T, Nidzworski D, Olszewski M, Gromadzka B. Ultra-Selective and Sensitive Fluorescent Chemosensor Based on Phage Display-Derived Peptide With an N-Terminal Cu(II)-Binding Motif. Biosensors. 2024;14(11):555.
122. Daniels BE, Stivala CE. A Solid-Phase Approach for the Synthesis of A-Aminoboronic Acid Peptides. RSC Advances. 2018;8(6):3343-7.
123. Moreno MR, Johnson NC, Stewart CB, Setelin ML, Wayment AX, Felix BM, Burt S C, Michaelis D J, Solid-Phase Peptide Synthesis and 2D NMR Analysis of Unknown Tripeptides: An Advanced Undergraduate Synthesis and Spectroscopy Laboratory. Journal of Chemical Education. 2024;101(5):2059-64.
124. Liang B, Li R, Li L, Tang M, Li X, Su C, Liao H, Silver-Promoted Solid-Phase Guanidinylation Enables the First Synthesis of Arginine Glycosylated Samoamide a Cyclopeptide Analogue. Frontiers in Chemistry. 2023;10.

125. Hameed DS, Sapmaz A, Gjonaj L, Merkx R, Ovaa H. Enhanced Delivery of Synthetic Labelled Ubiquitin Into Live Cells by Using Next-Generation Ub–TAT Conjugates. Chembiochem. 2018;19(24):2553-7.
126. Varró N, Erdei E, Bogdán D, Kalydi E, Deme R, Balogh B, Szigyártó I. Cs, Beke-Somfai T, Varga Z, Szabó P, Mándity I. Chemistry Open 2025; doi.org/10.1002/open.202500340
127. Varró N, Mándityné Huszka B, Erdei E, Mándoki A, Mándity I. Chemistry Methods. 2025; 00:e202500010. doi.org/10.1002/cmtd.202500010

9. Bibliography of the candidate's publications

9.1. Publications related to the thesis

1. N. Varró, B. Mándityné Huszka, E. Erdei, A. Mándoki, I. Mándity
   Upscaled synthesis of α- and β-peptides in a continuous-flow reactor using propylene carbonate as an eco-friendly solvent
   Chemistry Methods (2025)
   DOI: doi.org/10.1002/cmtd.202500010
2. I. Mándity, N. Varró, E. Erdei, D. Bogdán, E. Kalydi, R. Deme, B. Balogh, I. Cs. Szigyártó, T. Beke-Somfai, Z. Varga, P. Szabó
   Betaine-Conjugated ß-Peptide Foldamers, Influence of Quaternary Charge on Self-Organization and Morphology Formation
   Chemistry Open (2025)
   DOI: 10.1002/open.202500340

9.2. Other publications – not related to the thesis

1. I. Mándity, E. Erdei, J. Marcos, N. Varró, B. Bacsa, K. Horváti
   Spatiotemporal Control in Biomedicine: Photoswitchable Peptides and Foldamers
   British Journal of Pharmacology (2025)
2. B. Balogh, D. Bogdán, A. Czompa, R. Deme, P. Dunkel, Z. Kaleta, N. Kormosné Varró, G. Krajsovszky, I. Mándity, P. Pollák, L. Szabó
   Szerves kémia szemináriumok II.
   Budapest, Magyarország: Semmelweis Egyetem (2024)
   ISBN: 9786155722363
   Közlemény: 35084700 Admin láttamozott Forrás Könyv (Oktatási anyag) Oktatási
3. B. Balogh, D. Bogdán, A. Czompa, R. Deme, P. Dunkel, Z. Kaleta, N. Kormosné Varró, G. Krajsovszky, I. Mándity, P. Pollák
   Szerves kémia szemináriumok I.
   Budapest, Magyarország: Semmelweis Egyetem (2023)
   ISBN: 9786155722301
   Közlemény: 34433118 Admin láttamozott Forrás Könyv (Oktatási anyag) Oktatási

4. A. Mirzahosseiniz, M. Molaei, K. Mazák, T. Pálla, I. Köteles, N. Varró, I. Mándity, B. Noszál
   Species-specific acid-base characterization of carnosine and homocarnosine using nuclear magnetic resonance
   Chemical Physics Letters 808 Paper: 140128, 6 p. (2022)
5. L. Petri, P. Ábrányi-Balogh, D. Vagrys, T. Imre, N. Varró, I. Mándity, A. Rácz, L. Wittner, K. Tóth, E. Zs. Tóth, T. Juhász, B. Davis, Gy. M. Keserű
   A covalent strategy to target intrinsically disordered proteins: Discovery of novel tau aggregation inhibitors
   European Journal of Medicinal Chemistry 231 Paper: 114163, 13 p. (2022)
6. B. Nizami, D. Bereczki-Szakál, N. Varró, K. el Battioui, V. U Nagaraj, I. Cs. Szigyártó, I. Mándity, T. Beke-Somfai
   FoldamerDB: a database of peptidic foldamers
   Nucleic Acids Research 48: D1 pp. D1122-D1128. (2020)
7. K. Nemeth, N. Varro, B. Reti, P. Berki, B. Adam, K. Belina, K. Hernadi
   Synthesis and investigation of SiO2-MgO coated MWCNTs and their potential application
   Scientific Reports 9 Paper: 15113, 11 p. (2019)

10. Acknowledgements

First of all, I would like to thank my supervisor, Dr. István Mándity for providing the conditions and professional support for my PhD thesis.

I would also like to thank Prof. Dr. Romana Zelkó, head of the Doctoral School of Pharmaceutical Sciences, for following the progress of my PhD thesis and supporting its successful completion.

I would also like to thank my colleagues, Beáta Mándityné Huszka and Ilona Fülöpné Botos for their help, Imola Szigyártó who helped me a lot with DLS, CD and FT-IR studies at the Natural Sciences Research Centre. Additionally, gratitude is extended to Eszter Erdei for her help and support, Dóra Bogdán and Eszter Kalydi for NMR measurements and the other colleagues at the Institute of Organic Chemistry at Semmelweis University for their help and constructive professional discussions.

Thank you to my friends for their encouragement and help.

I would like to express my gratitude to my family, who have been steadfastly by my side and supported me in sometimes difficult moments.

Chemistry—Methods

Research Article
doi.org/10.1002/cmtd.202500010

Chemistry Europe
European Chemical Societies Publishing

www.chemistrymethods.org

Upscaled Synthesis of α- and β-Peptides in a Continuous-Flow Reactor Using Propylene Carbonate as an Eco-Friendly Solvent

Nikolett Varró, Beáta Mándityné Huszka, Eszter Erdei, András Mándoki, and István M. Mándity*

A rapid, eco-friendly, and scalable continuous-flow solid-phase peptide synthesis (CF-SPPS) technology has been developed using propylene carbonate (PC) as a solvent. PC, a greener alternative to DMF, is selected based on the GSK solvent selection guide. To evaluate its compatibility with CF-SPPS, four α-peptides were synthesized, achieving high yields and purity. The method is further validated with challenging sequences, including four β-peptide foldamers and an α/β-peptide chimera. To scale up this innovative approach, larger column geometries are optimized to ensure the appropriate resin load and flow rate for desired residence times. The technology demonstrated its capability to synthesize peptides on a >4 g scale with satisfactory efficiency. A key feature is the use of PC in minimal amounts, significantly enhancing the process's green credentials. The low solvent consumption and high efficiency align with green chemistry principles, reducing waste and improving sustainability. The low process mass intensity of the method highlights its environmental benefits, making it a sustainable alternative for large-scale peptide synthesis. This breakthrough showcases the potential of CF-SPPS with PC as a solvent to meet the demands of greener and more efficient peptide production.

1. Introduction

Flow reactions have garnered significant attention in recent years due to their numerous advantages over traditional batch processes.[1–5] As a dynamic and innovative approach, flow chemistry addresses many limitations of conventional synthesis methods, making it a highly attractive option for both academic research and industrial applications.[6–13]

Flow chemistry offers enhanced control over reaction conditions, allowing accurate temperature and pressure regulation, which leads to improved reaction rates and yields.[14–16] The continuous nature of flow reactions minimizes the handling of hazardous materials, significantly reducing safety risks.[14,17–22] Furthermore, the scalability of flow processes from laboratory to industrial production facilitates seamless transitions and consistent product quality.[4,18,23–25]

The synthesis of peptides, crucial in the production of pharmaceuticals[26–28] and in biochemistry,[28–36] has traditionally relied on hazardous solvents and inefficient batch processes.[37–41] Recently, flow chemistry has emerged as a sustainable alternative in the field of solid-phase peptide synthesis (SPPS), too.[2,36,42–45] Flow-based SPPS allows rapid peptide synthesis with high purity, significantly reducing the time required for synthesis and cutting down the amount of reagents and solvents needed.[3,46–57] Process mass intensity (PMI)[58] is a crucial metric in peptide synthesis[59] as it quantifies the efficiency and environmental impact of the process by measuring the total mass of materials used relative to the final product mass. A low PMI indicates a greener, more sustainable synthesis, aligning with modern principles of green chemistry and minimizing waste generation in large-scale peptide production. The advancement of continuous-flow solid-phase peptide synthesis (CF-SPPS) is pivotal in the context of green chemistry, as it aligns with the principles of reducing the usage of hazardous chemicals and increasing process efficiency.[60]

The integration of green technologies[61] and solvents into chemical synthesis processes is of considerable current interest.[62,63] Propylene carbonate (PC) is considered to be a green solvent[64–66] due to its environmentally friendly properties and its sustainable production process. It is synthesized through the reaction of propylene oxide with carbon dioxide, which helps mitigate greenhouse gas emissions by utilizing CO_2.[67,68] This reaction not only reduces atmospheric CO_2 but results in a solvent with low toxicity as well, making the process safer for both human health and the environment.[69] Additionally, its low volatility minimizes harmful volatile organic compound emissions.

N. Varró, E. Erdei, A. Mándoki, I. M. Mándity
Department of Organic Chemistry
Semmelweis University
Hőgyes Endre utca 7., 1092 Budapest, Hungary
E-mail: mandity.istvan@semmelweis.hu

N. Varró, B. Mándityné Huszka, E. Erdei, A. Mándoki, I. M. Mándity
Institute of Materials and Environmental Chemistry
HUN-REN Research Centre for Natural Sciences
Magyar tudósok körútja 2., 1117 Budapest, Hungary

B. Mándityné Huszka
Ladon Therapeutics Inc
Szőregi ut 38, H-6726 Szeged, Hungary

Supporting information for this article is available on the WWW under https://doi.org/10.1002/cmtd.202500010

Despite these advantages, PC has not yet been widely adopted in flow chemical synthesis. Herein we aim 1) to integrate PC to CF-SPPS and 2) to develop an upscaled CF process for the gram-scale synthesis of peptides.

2. Results and Discussion

A continuous-flow (CF) reactor was used in this study (**Figure 1**), consisting of an high performance liquid chromatography (HPLC) Reo autosampler, an HPLC column thermostat with a stainless-steel column, a semi-preparative HPLC pump, a back-pressure regulator, and a line selection valve system. This setup permitted the recirculation of the reagent mixture on the resin bed. The HPLC autosampler allowed reproducible and precise mixing and injection of the reagents needed for peptide synthesis. The HPLC pump offered the pulse-free delivery of the liquids. The resin on which the peptide chain was grown was filled into a stainless steel column, and then, the latter was heated by an HPLC thermostat to the desired temperature. To maintain a constant pressure for the system, a back-pressure regulator was applied, thereby keeping the pressure constant.

A major aim was to replace the hazardous DMF solvent with a greener alternative. Our choice was the use of a PC. A comprehensive screening and fine-tuning of reaction parameters were carried out using compound 1 as a test sequence, and the purity of the crude product was assessed throughout the optimization. First, we investigated the temperature dependence of the coupling reaction. As shown in Table S3 Supporting Information, the highest coupling efficiency was achieved at 70 °C. Next, we examined the pressure dependence at this temperature. At 60 bar, the crude purity reached 96% (Table S4, Supporting Information), and further increases in pressure did not improve the outcome. The effect of amino acid equivalents was also evaluated. As shown in Table S5, Supporting Information, reducing the amount of amino acid led to unacceptably low crude purities. To accelerate the synthesis, the flow rate was fine tuned. Results in Table S6, Supporting Information, indicate that a high crude purity could still be maintained at a flow rate of 0.3 mL min^{-1}. Finally, to reduce solvent consumption in the CF system, the concentration of the coupling mixture was optimized. As shown in Table S7, Supporting Information, excellent crude purity was retained at 100 mM concentration, corresponding to 0.1 mmol amino acid dissolved in 1 mL of PC. The established conditions were consistently applied in all synthetic operations. Namely, the thermostat was set to 70 °C, the back-pressure regulator to 60 bars, and the residence time was kept at 5 min with a flow rate of 0.3 mL min^{-1}. The stainless-steel column with a length of 25 cm was filled with 300 mg of Tenta Gel R RAM resin. Importantly, only 1.5 equiv. of amino acids was used with 1.5 equiv. active ester forming ethyl cyanoglyoxylate-2-oxime (OxymaPure) as a coupling agent in the presence of 1.5 equiv. *N,N*-diisopropylcarbodiimide (DIC). The mixing of the reagents was carried out by the autosampler. For the deprotection, 2% piperidine and 2% 1,8-diazabicyclo[5.4.0]undec-7-ene (DBU) were used in PC. Between the two steps, a washing period was applied for 5 min with PC.

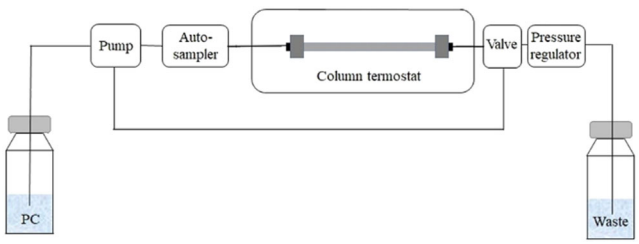

Figure 1. Schematic illustration of the CF apparatus used. PC was used during the synthesis. This system consists of an HPLC pump, an autosampler, a column thermostat, a flow-line selection valve system, and a pressure regulator.

To test the setup described above, first, a simple α-peptide (**1**) was synthesized. After the completion of the coupling of the peptide chain, the resin was removed from the column, and an offline cleavage was performed under regular conditions. The raw peptide, after lyophilization, was analyzed by HPLC-MS technique. As shown in **Table 1**, impressive results were gained for compound **1**, with an isolated yield of 96% and a raw purity of >98%. On the basis of this promising finding, the CF setup was tested on three additional α-peptide sequences (**2**, **3,** and **4**) with considerable biomedical potential. Compounds **2** and **4** are antimicrobial peptides (DHVAR-4 and PGLA, respectively), while **3**, called penetratin, is a cell-membrane penetrating peptide.[70] The optimized CF-SPPS technique confirmed our aims for a fast and effective synthesis. In all cases, high yields and excellent raw purities were obtained (Table 1, entries 2–4), which supports the effectiveness of the CF reaction setup with PC as solvent.

Since coupling efficiencies were acceptable for longer peptide chains containing 21 amino acids, too, the optimized technology was tested on more difficult sequences such as β-peptides.[71–73] The coupling of β-amino acids requires special coupling reagents such as 1-[bis(dimethylamino)methylene]-1*H*-1,2,3-triazolo[4,5-b]pyridinium 3-oxide hexafluorophosphate (HATU) along with *N,N*-diisopropylethylamine (DIPEA) as base. However, once HATU and DIPEA were mixed in PC, some minor precipitation occurred, blocking the tubing of the reactor. Thus, to avoid precipitation, the previously used reagents, OxymaPure in combination with DIC, were used. Because of the difficulty of coupling β-amino acids, the reagents were recirculated on the column by switching the valve system into recycling mode. The recycling time was set to 30 min for both couplings and deprotections. The latter step was applied to avoid the potentially incomplete removal of Fmoc,[74] known for β-peptide oligomers.[75–77] With this procedure, recycling the reagent on the resin bed, β-peptides **5**–**8** and α/β-peptide **9** were successfully

Table 1. Results of the synthesized α-peptides using PC as solvent at a 0.07 mmol scale.

Entry	Compound	Sequence of the peptide with one-letter code	Raw purity [%]	Yield [%]
1	**1**	ALFEK-NH_2	>98	96
2	**2**	KRLFKKLLFSLRKY-NH_2	>96	94
3	**3**	RQIKIWFQNRRMKWKK-NH_2	>97	93
4	**4**	GMASKAGAIAGKIAKVALKAL-NH_2	>95	91

Research Article
doi.org/10.1002/cmtd.202500010
Chemistry Europe
European Chemical Societies Publishing

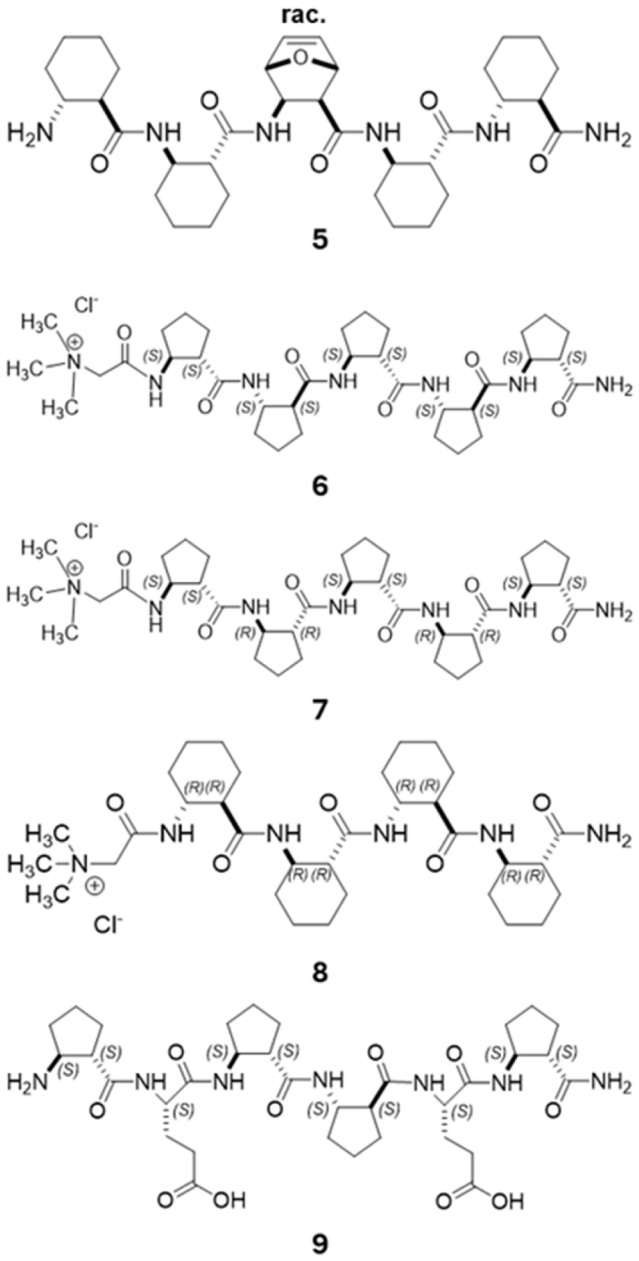

Scheme 1. Structures of the synthesized β-peptide foldamers using PC as solvent at a 0.07 mmol scale.

Table 2. Results of the synthesized β-peptide foldamers using PC as solvent at a 0.07 mmol scale.

Entry	Compound	Raw purity [%]	Yield [%]
1	**5**	>96	89
2	**6**	>97	87
3	**7**	>98	86
4	**8**	>98	91
5	**9**	>98	93

synthesized (**Scheme 1**, **Table 2**). After the completion of the coupling of the amino acids, the peptides were cleaved offline, and the raw materials were analyzed after lyophilization.

The results indicated that excellent raw purities and good to excellent yields were achieved for compounds **5–9** as well. Representative HPLC-MS chromatograms are shown in **Figure 2**, which strongly support the high purity of the raw materials obtained after ethereal precipitation.

The direct comparison of the time required for the peptide-chain coupling under classic SPPS conditions and under CF-SPPS conditions carried out in PC shows a drastic difference (**Table 3**). The scale and reagent concentrations were identical in both cases. For manual SPPS, coupling and deprotection times were based on literature data.[78] The synthesis in CF is considerably faster in PC than those reachable for classic SPPS conditions.

A considerable advantage of the developed method, besides the use of PC as solvent, is the amount of the solvent utilized; namely, it is minimal compared to regular technologies (**Table 4**).

The results support the view that the CF-SPPS technology utilizes solvent in about two orders of magnitude lower quantity than those for classic SPPS methodologies.

To exactly estimate the effectiveness of the developed technology, PMI values were calculated for the classic SPPS and for the CF-SPPS conditions. Importantly, the PMI value reflects not only the solvent used, but also the amount of building blocks and amino acids incorporated too. The results are summarized in **Table 5**.

For all the investigated compounds, the PMI value under classical SPPS conditions exceeds 10 000. In contrast, under optimized CF-SPPS conditions, the PMI value ranges between 434 and 693. These significantly lower values not only represent a substantial improvement over classical SPPS but also approach the efficiency levels observed in the synthesis of small organic drug molecules. This improvement underscores the potential for peptides to be utilized as viable drug candidates in the near future.

A further aim was to upscale the CF-SPPS synthesis by the use of HPLC columns with larger filling capacity. Based on our previous results[49,53] and the geometries of the larger columns, calculations were carried out (Table 5) to determine the required amount of resin to completely and evenly fill the column and the necessary flow rate to maintain the 5 min residence time, parameters crucial for successful CF peptide synthesis. For the scale-up study, two columns of different diameters were used, both with a length of 250 mm. Specifically, the column diameter was 10 mm (Table 5, entry 2) or 20 mm (Table 5, entry 3), allowing for significantly larger synthesis scales of 0.375 mmol and 1.5 mmol, respectively. According to published results for the 4 mm-wide column with a length of 250 mm, 300 mg of resin was suitable. With a flow rate of 0.3 mL min^{-1}, the residence time was kept at 5 min. For the larger columns, first, their volumes were calculated. Knowing the mass and volume of the resin to be filled in, subtracting the volume of the resin from the volume of the column, the dead volume of the resin bed, filled with the solvent under synthetic runs, could be calculated. If this volume is divided by the 5 min residence time, the flow rate to be used can be determined. The scale of the synthesis was calculated from the mass of the filled resin, which was multiplied by the 0.2 mmol g^{-1} loading of the TentaGel RRAM resin. The results are summarized in Table S8, Supporting Information.

Research Article
doi.org/10.1002/cmtd.202500010
Chemistry Europe
European Chemical Societies Publishing

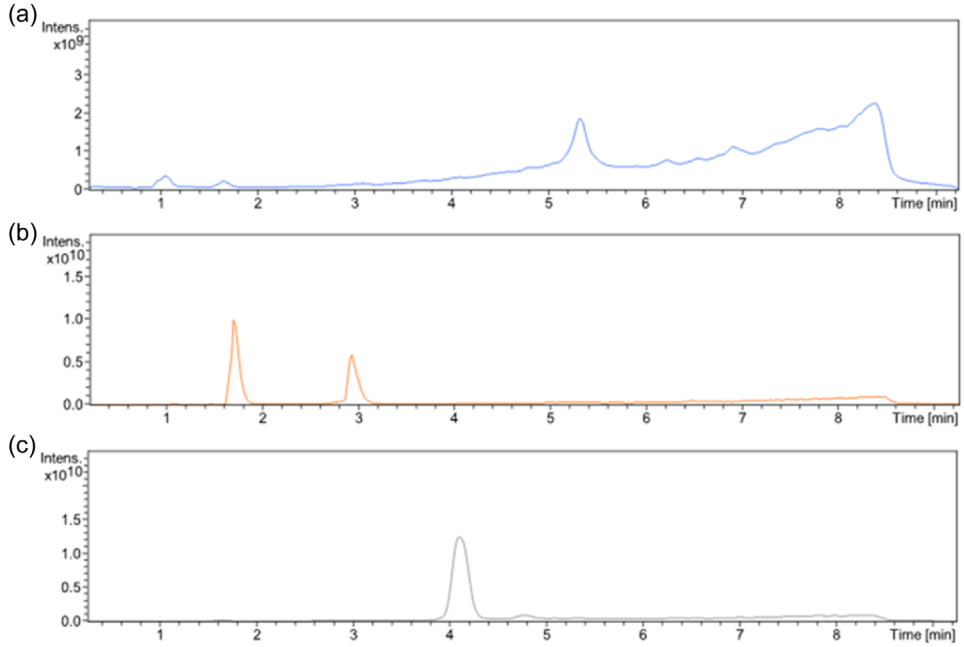

Figure 2. HPLC-MS chromatograms of the raw material of α-peptides a) **1** and b) **3**, as well as c) β-peptide **6**, synthesized in CF-SPPS using PC as solvent at a 0.07 mmol scale.

Table 3. Comparison of the time needed for the complete peptide chain assembly under the classic SPPS and the CF-SPPS conditions using PC as solvent at a 0.07 mmol scale.

Compound	Classic SPPS [min][a)]	CF-SPPS [min][b)]
1	≈820	≈124
2	≈2260	≈334
3	≈2580	≈381
4	≈3380	≈498
5	≈1120	≈357
6 and **7**	≈2560	≈427
8	≈2340	≈357
9	≈1100	≈240

[a)]Coupling time: 120 min, deprotection: 20 min, washing 20 min. [b)]Coupling time for **1–4** and for **5–9**: 6.7 min and 30 min respectively, deprotection time for **1–4** and for **5–9**: 6.7 and 30 min respectively, washing 10 min

Table 4. Comparison of the solvent used for the complete peptide chain assembly under the classic SPPS and under the CF-SPPS conditions, carried out in PC as solvent at a 0.07 mmol scale.

Compound	Solvent used for peptide chain synthesis [mL]	
	Classic SPPS	CF-SPPS
1	≈1680	≈18.5
2	≈4650	≈50.1
3	≈5310	≈57.2
4	≈6960	≈74.7
5	≈1680	≈18.6
6 and **7**	≈2010	≈22.1
8	≈1680	≈18.6
9	≈2010	≈22.1

Table 5. Comparison of PMI values for classic SPPS and under the CF-SPPS conditions carried out in PC as solvent at a 0.07 mmol scale.

Compound	PMI value for classic SPPS	PMI value for classic SPPS per AA residue	PMI value for CF-SPPS	PMI value for CF-SPPS per AA residue
1	58 027	11 605	658	132
2	39 370	2812	434	31
3	51 062	3191	564	35
4	63 326	3016	693	33
5	57 895	11 579	659	132
6 and **7**	66 279	11 046	757	126
8	56 768	9461	658	110
9	60 302	10 050	681	113

Table 6. Results of the synthesis of CF-SPPS carried out with a column with a diameter and length of 10 and 250 mm at a scale of 0.375 mmol.

Compound	Isolated amount of peptide [mg]	Raw purity	Yield	Solvent used [mL]	Time needed [min]	PMI
2	794	>96%	84	≈626.8	≈334	434
3	993	>97%	87	≈714.6	≈381	564
4	782	>95%	86	≈933.9	≈498	693

Table 7. Results of CF-SPPS synthesis carried out with a column possessing a diameter and length of 20 and 250 mm at a scale of 1.5 mmol.

Compound	Isolated amount of peptide [mg]	Raw purity	Yield	Solvent used [mL]	Time needed [min]	PMI
3	4154	>97%	91	≈2858.3	≈334	564

Research Article
doi.org/10.1002/cmtd.202500010
Chemistry Europe
European Chemical Societies Publishing

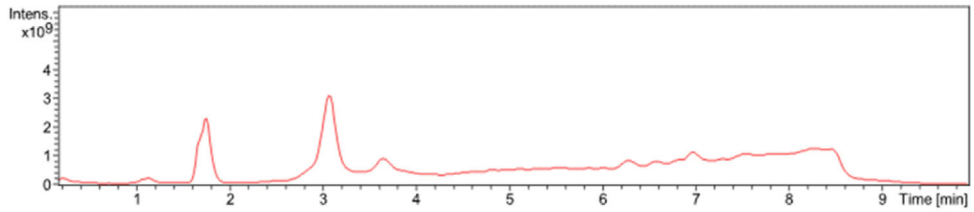

Figure 3. HPLC-MS chromatogram of the >4 g raw material of **3** synthesized at a scale of 1.5 mmol.

To test the validity of the calculations, three α-peptides (**2**, **3,** and **4**) with considerable biomedical applications were synthesized on a scale of 0.375 mmol using the column with a diameter of 10 mm. The results of the performed syntheses are shown in **Table 6**.

In all cases, good yields were gained with high raw purity. Importantly, peptides close to the gram scale were isolated with a peptide chain construction time of 5–8 h. Outstandingly, the solvent used again was PC, and the required amount of solvent is measured in milliliters rather than in liters, that is, with a quantity one order of magnitude lower than those for classic SPPS.

To further challenge the designed scale-up setup, the synthesis of **3** (penetratin) was carried out in the column with a length and diameter of 250 and 20 mm, respectively. The results are summarized in **Table 7** and the representative HPLC-MS chromatogramm is shown in **Figure 3**.

Notably, >4 g of penetratin peptide were isolated in less than a synthesis time of 6 h. Again, the solvent was PC, and >4 g of peptide was synthesized by the use of <3 L PC.

For both scales of the upscaled syntheses, the PMI values remained consistent due to the linear nature of the scale-up process. The PMI values, ranging between 434 and 693, are comparable to those observed in the synthesis of small organic drug molecules, further underscoring their potential for utilization as drug candidates in the pharmaceutical industry.

3. Conclusion

In summary, a rapid, green, highly efficient, and upscaled CF-SPPS technology has been developed for the synthesis of various peptides and foldamers in PC as solvent. Our first aim was to replace DMF with a more eco-friendly solvent, like PC, which is considered the ultimate choice according to the GSK solvent selection guide. To test the compatibility of PC with CF-SPPS, four different α-peptides were synthesized in high yields with raw purity. The efficiency of the CF-SPPS technology was further demonstrated with the synthesis of difficult sequences, like four different β-peptide foldamers and an α/β-peptide chimera, with great success. A further goal was to upscale this new methodology. A calculation was made according to the geometric parameters of larger columns to estimate the necessary amount of the resin to be filled and the flow rate to be used to obtain the aimed residence time. The scale-up was carried out in steps, and the technology showed efficient production of peptides even on a >4 g scale. Noteworthy property of the system is the use of PC as a solvent. More importantly, the amount of solvent used is remarkably low. Notably, for both small-scale and gram-scale peptide syntheses, the PMI values remained consistent, ranging between 434 and 693, comparable to those observed in the synthesis of conventional small organic molecules. These features make the developed technology exceptionally green and efficient, potentially paving the way for greater utilization of peptides in drug development and the pharmaceutical industry.

4. Experimental Section

Peptide Synthesis

Peptide chains were synthesized on Tentagel R RAM resin using 1.5 equiv of Fmoc-protected amino acids with 1.5 equiv of DIC and OxymaPure as coupling reagents in PC at a concentration of 100 mM. Reactions were optimized at 60 bar, 70 °C, with a 5 min residence time and automatic recirculation for β-amino acids for 30 min. Deprotection was carried out using 2% DBU and 2% piperidine in PC, with 5 min PC washes between steps.

Peptide Cleavage

Peptides were cleaved from the resin using a solution of 90% TFA, 2.5% DTT, 2.5% TIPS, and 5% water. The cleavage process started in an ice bath and proceeded to room temperature over 4 h. TFA was evaporated with nitrogen gas, and the peptides were precipitated in cold diethyl ether, filtered, dissolved in 5% acetic acid, and lyophilized.

Analysis

Crude peptides were analyzed by RP-HPLC-MS using an Aeris PEPTIDE XB-C18 column with a gradient of 5–80% acetonitrile (containing 0.1% formic acid) over 7 min, followed by a 3 min re-equilibration. Peptides **1–4** were analyzed using the same gradient, extended over 25 min. The system included an Agilent 1200 HPLC and a Bruker HCTultra ETD II mass spectrometer. Additionally, 1H NMR measurements were performed using a Varian Mercury Plus 400 MHz NMR spectrometer.

Acknowledgements

The authors are grateful to the Hungarian Research Foundation (OTKA ANN 139484). The financial support of the National Research, Development and Innovation Office (GYORSÍTÓSÁV-2021-00009, TKP2021-EGA-31) is acknowledged. Project no. RRF-2.3.1-21-2022-00015 has been implemented with support

provided by the European Union. E.E. and A.M. acknowledge the grant of EFOP-3.6.3-VEKOP-16-2017-00009.

Conflict of Interest

The authors declare no conflict of interest.

Data Availability Statement

The data that support the findings of this study are available in the supplementary material of this article.

Keywords: continuous flow · green · peptide · propylene carbonate · synthesis

[1] L. Capaldo, Z. Wen, T. Noël, *Chem. Sci.* **2023**, *14*, 4230.
[2] H. Masui, S. Fuse, *Org. Process Res. Dev.* **2022**, *26*, 1751.
[3] C. Li, A. J. Callahan, M. D. Simon, K. A. Totaro, A. J. Mijalis, K.-S. Phadke, G. Zhang, N. Hartrampf, C. K. Schissel, M. Zhou, H. Zong, G. J. Hanson, A. Loas, N. L. B. Pohl, D. E. Verhoeven, B. L. Pentelute, *Nat. Commun.* **2021**, *12*, 4396.
[4] K. F. Jensen, *AIChE J.* **2017**, *63*, 858.
[5] I. M. Mándity, S. B. Ötvös, G. Szőllősi, F. Fülöp, *Chem. Rec.* **2016**, *16*, 1018.
[6] F. Nuti, C. Gellini, M. Larregola, L. Squillantini, R. Chelli, P. R. Salvi, O. Lequin, G. Pietraperzia, A. M. Papini, *Front. Chem.* **2019**, *7*.
[7] C. Wiles, P. Watts, *Green Chem.* **2012**, *14*, 38.
[8] R. L. Hartman, K. F. Jensen, *Lab Chip* **2009**, *9*, 2495.
[9] Y. Zhang, S. C. Born, K. F. Jensen, *Org. Process Res. Dev.* **2014**, *18*, 1476.
[10] N. Kockmann, M. Gottsponer, D. M. Roberge, *Chem. Eng. J.* **2011**, *167*, 718.
[11] J. H. A. Schuurmans, T. M. Masson, S. D. A. Zondag, P. Buskens, T. Noël, *ChemSusChem* **2024**, *17*, e202301405.
[12] A. A. H. Laporte, T. M. Masson, S. D. A. Zondag, T. Noël, *Angew. Chem. Int. Ed.* **2024**, *63*, e202316108.
[13] A. Hyer, D. Gregory, K. Kay, Q. Le, J. Turnage, F. Gupton, J. K. Ferri, *Adv. Synth. Catal.* **2024**, *366*, 357.
[14] M. Movsisyan, E. I. P. Delbeke, J. K. E. T. Berton, C. Battilocchio, S. V. Ley, C. V. Stevens, *Chem. Soc. Rev.* **2016**, *45*, 4892.
[15] M. B. Plutschack, B. Pieber, K. Gilmore, P. H. Seeberger, *Chem. Rev.* **2017**, *117*, 11796.
[16] M. Elsherbini, T. Wirth, *Acc. Chem. Res.* **2019**, *52*, 3287.
[17] D. T. McQuade, P. H. Seeberger, *J. Org. Chem.* **2013**, *78*, 6384.
[18] B. Gutmann, D. Cantillo, C. O. Kappe, *Angew. Chem., Int. Ed.* **2015**, *54*, 6688.
[19] J. C. Brandt, T. Wirth, *Beilstein J. Org. Chem.* **2009**, *5*.
[20] S. P. Green, K. M. Wheelhouse, A. D. Payne, J. P. Hallett, P. W. Miller, J. A. Bull, *Org. Process Res. Dev.* **2020**, *24*, 67.
[21] P. Bianchi, J.-C. M. Monbaliu, *Acc. Chem. Res.* **2024**, *57*, 2207.
[22] C. M. Pacheco, F. A. Lima, M. R. B. P. Gomez, L. B. Barbosa, R. A. C. Leão, R. O. M. A. de Souza, *J. Flow Chem.* **2024**, *14*, 491.
[23] N. Kaplaneris, M. Akdeniz, M. Fillols, F. Arrighi, F. Raymenants, G. Sanil, D. T. Gryko, T. Noël, *Angew. Chem. Int. Ed.* **2024**, *63*, e202403271.
[24] V. Hessel, D. Kralisch, N. Kockmann, T. Noël, Q. Wang, *ChemSusChem* **2013**, *6*, 746.
[25] A. Isidro-Llobet, M. N. Kenworthy, S. Mukherjee, M. E. Kopach, K. Wegner, F. Gallou, A. G. Smith, F. Roschangar, *J. Org. Chem.* **2019**, *84*, 4615.
[26] A. Gronewold, M. Horn, I. Ranđelović, J. Tóvári, S. Muñoz Vázquez, K. Schomäcker, I. Neundorf, *ChemMedChem* **2017**, *12*, 42.
[27] I. Gessner, I. Neundorf, *Int. J. Mol. Sci.* **2020**, *21*, 2536.
[28] J. Grabeck, J. Mayer, A. Miltz, M. Casoria, M. Quagliata, D. Meinberger, A. R. Klatt, I. Wielert, B. Maier, A. M. Papini, I. Neundorf, *ACS Infect. Dis.* **2024**, *10*, 2717.
[29] E. T. Sletten, M. Nuño, D. Guthrie, P. H. Seeberger, *Chem. Commun.* **2019**, *55*, 14598.
[30] A. Pandey, A. K. Goyal, *Pharm. Pat. Anal.* **2024**, 1.
[31] J. Zhang, M. Zhao, Y. He, Y. Dong, *J. Pept. Sci.* **2023**, *29*, e3452.
[32] J. Zhang, H. Xu, J. Lu, Y. Dong, J. Feng, *Bioorg. Med. Chem.* **2023**, *85*, 117291.
[33] A. D'Ercole, L. Pacini, G. Sabatino, M. Zini, F. Nuti, A. Ribecai, A. Paio, P. Rovero, A. M. Papini, *Org. Process Res. Dev.* **2021**, *25*, 2754.
[34] P. Strauss, F. Nuti, M. Quagliata, A. M. Papini, M. Hurevich, *Org. Biomol. Chem.* **2023**, *21*, 1674.
[35] L. Pacini, M. Muthyala, L. Aguiar, R. Zitterbart, P. Rovero, A. M. Papini, *J. Pept. Sci.* **2024**, *30*, e3605.
[36] G. Sabatino, A. D'Ercole, L. Pacini, M. Zini, A. Ribecai, A. Paio, P. Rovero, A. M. Papini, *Org. Process Res. Dev.* **2021**, *25*, 552.
[37] B. Shen, D. M. Makley, J. N. Johnston, *Nature* **2010**, *465*, 1027.
[38] R. Subiros-Funosas, R. Prohens, R. Barbas, A. El-Faham, F. Albericio, *Chem. Eur. J.* **2009**, *15*, 9394.
[39] C. A. Hood, G. Fuentes, H. Patel, K. Page, M. Menakuru, J. H. Park, *J. Pept. Sci.* **2008**, *14*, 97.
[40] B. Bacsa, B. Desai, G. Dibo, C. O. Kappe, *J. Pept. Sci.* **2006**, *12*, 633.
[41] G. Sabatino, B. Mulinacci, M. Alcaro, M. Chelli, P. Rovero, A. Papini, *Lett. Pept. Sci.* **2002**, *9*, 119.
[42] M. D. Simon, P. L. Heider, A. Adamo, A. A. Vinogradov, S. K. Mong, X. Li, T. Berger, R. L. Policarpo, C. Zhang, Y. Zou, X. Liao, A. M. Spokoyny, K. F. Jensen, B. L. Pentelute, *ChemBioChem* **2014**, *15*, 713.
[43] S. Mohapatra, N. Hartrampf, M. Poskus, A. Loas, R. Gómez-Bombarelli, B. L. Pentelute, *ACS Cent. Sci.* **2020**, *6*, 2277.
[44] K. E. Ruhl, M. J. Di Maso, H. B. Rose, D. M. Schultz, F. Lévesque, S. T. Grosser, S. M. Silverman, S. Li, N. Sciammetta, U. F. Mansoor, *Org. Process Res. Dev.* **2024**, *28*, 2896.
[45] L. Ferrazzano, M. Catani, A. Cavazzini, G. Martelli, D. Corbisiero, P. Cantelmi, T. Fantoni, A. Mattellone, C. De Luca, S. Felletti, W. Cabri, A. Tolomelli, *Green Chem.* **2022**, *24*, 975.
[46] I. Nekkaa, D. Bogdán, T. Gáti, S. Béni, T. Juhász, M. Palkó, G. Paragi, G. K. Tóth, F. Fülöp, I. M. Mándity, *Chem. Commun.* **2019**, *55*, 3061.
[47] A. Szloszár, I. M. Mándity, F. Fülöp, *J. Flow Chem.* **2018**, *8*, 21.
[48] A. Szloszár, F. Fülöp and I. M. Mándity, *ChemistrySelect* **2017**, *2*, 6036.
[49] I. M. Mándity, B. Olasz, S. B. Ötvös, F. Fülöp, *ChemSusChem* **2014**, *7*, 3172.
[50] K. Ferentzi, D. Nagy-Fazekas, V. Farkas, A. Perczel, *React. Chem. Eng.* **2024**, *9*, 58.
[51] V. Goldschmidt Gőz, K. H. Y. Duong, D. Horváth, K. Ferentzi, V. Farkas, A. Perczel, *Eur. J. Org. Chem.* **2021**, *2021*, 6071.
[52] V. Farkas, K. Ferentzi, K. Horváti, A. Perczel, *Org. Process Res. Dev.* **2021**, *25*, 182.
[53] S. Szaniszló, K. Ferentzi, A. Perczel, V. Farkas, *Org. Process Res. Dev.* **2023**, *27*, 1053.
[54] B. Tamás, P. L. Willi, H. Bürgisser, N. Hartrampf, *React. Chem. Eng.* **2024**, *9*, 825.
[55] E. T. Williams, K. Schiefelbein, M. Schuster, I. M. M. Ahmed, M. De Vries, R. Beveridge, O. Zerbe, N. Hartrampf, *Chem. Sci.* **2024**, *15*, 8756.
[56] K. Schiefelbein, J. Lang, M. Schuster, C. E. Grigglestone, R. Striga, L. Bigler, M. C. Schuman, O. Zerbe, Y. Li, N. Hartrampf, *J. Am. Chem. Soc.* **2024**, *146*, 17261.
[57] N. Hartrampf, A. Saebi, M. Poskus, Z. P. Gates, A. J. Callahan, A. E. Cowfer, S. Hanna, S. Antilla, C. K. Schissel, A. J. Quartararo, X. Ye, A. J. Mijalis, M. D. Simon, A. Loas, S. Liu, C. Jessen, T. E. Nielsen, B. L. Pentelute, *Science* **2020**, *368*, 980.
[58] C. Jimenez-Gonzalez, C. S. Ponder, Q. B. Broxterman, J. B. Manley, *Org. Process Res. Dev.* **2011**, *15*, 912.
[59] I. Kekessie, K. Wegner, I. Martinez, M. E. Kopach, T. D. White, J. K. Tom, M. N. Kenworthy, F. Gallou, J. Lopez, S. G. Koenig, P. R. Payne, S. Eissler, B. Arumugam, C. Li, S. Mukherjee, A. Isidro-Llobet, O. Ludemann-Hombourger, P. Richardson, J. Kittelmann, D. Sejer Pedersen, L. J. van den Bos, *J. Org. Chem.* **2024**, *89*, 4261.
[60] M. Poliakoff, J. M. Fitzpatrick, T. R. Farren, P. T. Anastas, *Science* **2002**, *297*, 807.
[61] S. Knauer, N. Koch, C. Uth, R. Meusinger, O. Avrutina, H. Kolmar, *Angew. Chem. Int. Ed.* **2020**, *59*, 12984.
[62] J. Pawlas, J. H. Rasmussen, *ChemSusChem* **2021**, *14*, 3231.
[63] J. Liao, R. Zhang, X. Jia, M. Wang, C. Li, J. Wang, R. Tang, J. Huang, H. You, F.-E. Chen, *Green Chem.* **2024**, *26*, 10549.
[64] T. Welton, *Proc. R. Soc. A* **2015**, *471*, 20150502.
[65] N. Winterton, *Clean Technol. Environ. Policy* **2021**, *23*, 2499.
[66] C. M. Alder, J. D. Hayler, R. K. Henderson, A. M. Redman, L. Shukla, L. E. Shuster, H. F. Sneddon, *Green Chem.* **2016**, *18*, 3879.
[67] S. Huang, J. Ma, J. Li, N. Zhao, W. Wei, Y. Sun, *Catal. Commun.* **2008**, *9*, 276.
[68] A. I. Adeleye, D. Patel, D. Niyogi, B. Saha, *Ind. Eng. Chem. Res.* **2014**, *53*, 18647.
[69] S. B. J. Forero, A. H. J. Muñoz, J. Junior Jones, M. d. F. Silva, *Curr. Org. Synth.* **2016**, *13*, 834.
[70] A. Imre, B. Balogh, I. Mándity, *Br. J. Pharmacol.* **2025**, *182*, 495.
[71] K. Möhle, R. Günther, M. Thormann, N. Sewald, H.-J. Hofmann, *Biopolymers* **1999**, *50*, 167.
[72] A. Rimkus, N. Sewald, *Org. Lett.* **2003**, *5*, 79.

[73] F. Schumann, A. Müller, M. Koksch, G. Müller, N. Sewald, *J. Am. Chem. Soc.* **2000**, *122*, 12009.
[74] B. D. Larsen, A. Holm, *Int. J. Pept. Protein Res.* **1994**, *43*, 1.
[75] P. I. Arvidsson, J. Frackenpohl, D. Seebach, *Helv. Chim. Acta* **2003**, *86*, 1522.
[76] T. B. Potocky, A. K. Menon, S. H. Gellman, *Journal of the American Chemical Society* **2005**, *127*, 3686.
[77] J. K. Murray, S. H. Gellman, *Org. Lett.* **2005**, *7*, 1517.
[78] I. M. Mandity, E. Weber, T. A. Martinek, G. Olajos, G. K. Toth, E. Vass, F. Fulop, *Angew. Chem. Int. Ed.* **2009**, *48*, 2171.

Manuscript received: January 21, 2025
Revised manuscript received: March 28, 2025
Version of record online: May 2, 2025

ChemistryOpen

Research Article
doi.org/10.1002/open.202500340

Chemistry Europe
European Chemical Societies Publishing

www.chemistryopen.org

Betaine-Conjugated ß-Peptide Foldamers: Influence of Quaternary Charge on Self-Organization and MorphologyFormation

Nikolett Varró, Eszter Erdei, Dóra Bogdán, Eszter Kalydi, Ruth Deme, Balázs Balogh, Imola Cs. Szigyártó, Tamás Beke-Somfai, Zoltán Varga, Pál Szabó, and István M. Mándity*

The modification of well-known β-peptide helices has been achieved by the application of N-terminal betaine conjugation. The 3D self-organization of oligomers formed by [1*S*,2*S*]-2-aminocyclopentanecarboxylic acid (ACPC), [1*R*,2*R*]-2-aminocyclohexanecarboxylic acid (ACHC), and an alternating heterochiral homooligomer of [1*S*,2*S*]-ACPC and [1*R*,2*R*]-ACPC was studied. Results of NMR, ECD, FT-IR, and molecular modeling showed that for [1*S*,2*S*]-ACPC pentamer (**1**), the betaine conjugation did not affect the folding to an H12 helix. In contrast, for the [1*R*,2*R*]-ACHC tetramer (**2**) betaine conjugation notably influenced the folding, and an H14 helix was observed instead of the expected H10 helix. In addition, this is the first observation of self-association for an H12 helix forming β-peptide. Based on TEM images, this association leads to vesicle morphologies. For the alternating heterochiral homooligomer [1*S*,2*S*]-ACPC and the [1*R*,2*R*]-ACPC pentamer (**3**), betaine conjugation enhances the solubility of the system. Moreover, the formation of an expected E-strand can be anticipated, since self-association was found in the form of a fibrin net-like structure in TEM images. Betaine conjugates described herein open a new area of bioactive peptide foldamer construction, since the introduced quaternary charges may lead to important receptor-ligand interactions, while potential material science applications can also be realized.

1. Introduction

In the realm of scientific inquiry, there exists a fascinating array of non-natural compounds with peptide-like characteristics, showcasing an impressive spectrum of structural variability and wide-ranging utility across diverse scientific disciplines.[1] Notably, β-peptides, characterized by their composition of β-amino acids, stand out as a particularly scrutinized subset within this landscape, representing artificial constructs renowned for their inherent self-organizing properties. Classified as foldamers,[2] these molecular entities possess an intriguing propensity to adopt stable 3D conformations even when consisting of relatively short sequences. Their versatility extends to the formation of various secondary structures, encompassing helices,[1d,1f,3] strands,[4] and intricate hairpins,[4b,4c,5] while also exhibiting a remarkable capacity for the assembly of higher-order tertiary architectures such as vesicles[1a,1e,3a,4d,6] and nanofibers.[4d,7]

In terms of interdisciplinary research, foldamers have emerged as focal points of considerable interest, captivating attention across a myriad of industrial sectors. Their versatile applications span various domains, ranging from biomedicine,[1d,1e,6f,8] where they exhibit promise in modulating protein–protein interactions,[9]

N. Varró, E. Erdei, D. Bogdán, E. Kalydi, R. Deme, B. Balogh, I. M. Mándity
Department of Organic Chemistry
Semmelweis University
Hőgyes Endre utca 7, 1092 Budapest, Hungary
E-mail: mandity.istvan@semmelweis.hu

N. Varró, E. Erdei, D. Bogdán, E. Kalydi, R. Deme, B. Balogh, I. M. Mándity
Artificial Transporters Research Group
Institute of Materials and Environmental Chemistry
HUN-REN Research Centre for Natural Sciences
Magyar tudósok, körútja 2, 1117 Budapest, Hungary

I. C. Szigyártó, T. Beke-Somfai
Biomolecular Self-assembly Research Group
Institute of Materials and Environmental Chemistry
HUN-REN Research Centre for Natural Sciences
Magyar tudósok körútja 2., H-1117 Budapest, Hungary

Z. Varga
Biological Nanochemistry Research Group
Institute of Materials and Environmental Chemistry
HUN-REN Research Centre for Natural Sciences
Magyar tudósok körútja 2, H-1117 Budapest, Hungary

Z. Varga
Department of Physical Chemistry and Materials Science
Faculty of Chemical Technology and Biotechnology
Budapest University of Technology and Economics
Műegyetem rkp., 3., H-1111 Budapest, Hungary

P. Szabó
MS Metabolomics Laboratory
Cetre for Structural Study
HUN-REN Research Centre for Natural Sciences
Magyar tudósok körútja 2, H-1117 Budapest, Hungary

Supporting information for this article is available on the WWW under https://doi.org/10.1002/open.202500340

to the forefront of nanotechnology,[7c,7d] where their manipulation drives advancements in material chemistry. Furthermore, their utility extends to surface recognition[8d,9b,10] within artificial self-assemblies, unlocking new avenues for exploration.

Delving deeper into their potential, foldamers unveil an intricate tapestry of functionalities that transcend traditional boundaries. These molecular architectures present themselves as catalysts[8b,11] and sensors,[12] poised to revolutionize chemical processes and analytical methodologies.

These examples emphasize the importance of the folding of β-peptides and self-assemblies thereof to fulfill material chemical and biomedical functions beyond those of natural oligomers. The folding of β-peptides has been fine-tuned by various technologies, like backbone stereochemistry[4a,4e,5a,13] and side-chain shape.[4b–d,6g,6h,14]

In some cases, betaine, a zwitterionic molecule, has been utilized to modulate properties of peptides and proteins, including stability, solubility, and bioactivity. Incorporating betaine moieties into peptide sequences can confer enhanced resistance to proteolytic degradation, whereas betaine-containing peptides exhibit enhanced aqueous solubility.[15]

Herein, we show that by the introduction of quaternary cationic charges to foldameric structures, fine-tuning of solubility, folding, and self-assembly is further feasible.

2. Results and Discussion

The two archetypes of β-peptide helices, the right-handed H12 helix formed by the [1*S*,2*S*]-2-aminocyclopentanecarboxylic acid (ACPC) homochiral homooligomers[16] and right-handed H10 helix formed by the [1*R*,2*R*]-2-aminocyclohexanecarboxylic acid (ACHC) homochiral tetramer[3a]-, are well characterized 3D constructs. Regarding the strand like structures, the alternating heterochiral homooligomers of [1*S*,2*S*]-ACPC and [1*R*,2*R*]-ACPC[4e] previously published are a good example. In this study, we equipped the abovementioned oligomers with N-terminal betaine; thus, betaine-conjugated homochiral pentamer of [1*S*,2*S*]-ACPC (**1**),betaine-conjugated [1*R*,2*R*]-ACHC tetramer (**2**), and betaine-conjugated alternating heterochiral homooligomers of [1*S*,2*S*]-ACPC and [1*R*,2*R*]-ACPC (**3**) were created. The structures of the investigated betainiated compounds are shown in **Scheme 1**.

The synthesis of oligomers **1–3** was carried out first under regular solid-phase peptide synthesis (SPPS) conditions. However, due to the bulky nature of betaine possessing the quaternary positive charge, the desired products were not isolated. To overcome this problem, continuous-flow solid-phase peptide synthesis (CF-SPPS) was utilized.[17] This technique allows the use of low amino acid excesses, while complete conversion can be gained. It was already tested for the synthesis of β-peptides,[13c] however not for the coupling of bulky betaine on sterically hindered β-amino acids. Under optimized conditions, compounds **1–3** were isolated in >96% crude purity and >91% yields.

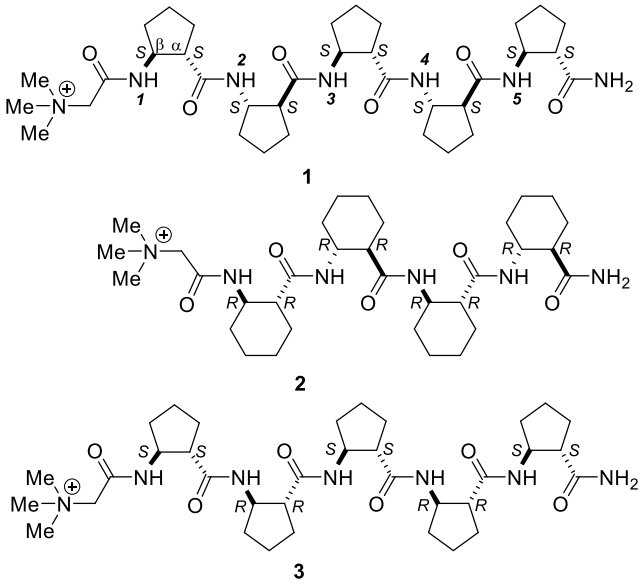

Scheme 1. The chemical structures of betaine-conjugated foldamers

First, the 3D organization of oligomers **1–3** were assessed by the NH/ND exchange measured by a series of 1H NMR spectra in CD_3OD in 4 mM concentration at 297 K. For oligomer **1** the time dependence of the residual NH signal intensities point to the fact that the corresponding atoms being considerably shielded from the solvent, due to the H-bonding interactions (**Figure 1**).

Proton resonances belonging to the C-terminal amide disappeared immediately after dissolution, while other signals remained for a longer period of time. The exchange pattern observed is in good accordance with the structure.[6g] The slowest exchange pattern was observed for NH^2. It is in the center of the helix, which shields considerably the proton from the solvent. NH^2 is followed by NH^1 and NH^3. The result of NH^3 is not surprising, since a proton is still in the middle of the structure. The slow exchange of NH^1, in turn, is somehow unexpected. However, it can be explained by the shielding effect of the bulky betaine part close to NH^1. A considerably faster exchange was observed for

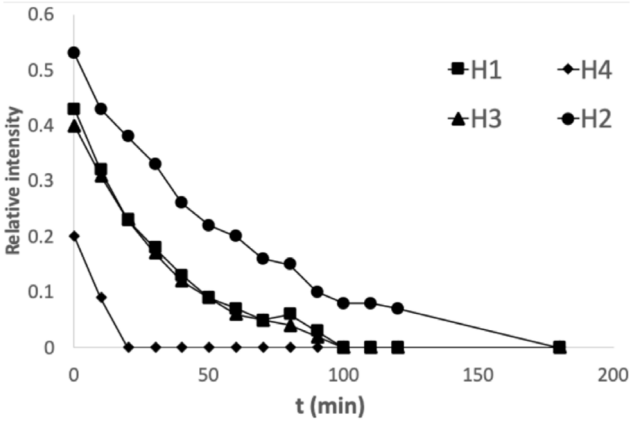

Figure 1. Time dependence of the NH/ND exchange for 4 mM solutions of **1** in CD_3OD.

NH^4, while NH^5 disappeared immediately after dissolution. This exchange pattern predicts the formation of an H12 helix, nonetheless, it is influenced by the self-association of the helices and by the bulky nature of the N-terminal betaine moiety.

For **2**, considerably slower exchange was observed. Namely, within 2 weeks, only 5–10% exchange was detected, and complete exchange was not reached even within 2 months. This result does not support the formation of an H10 helix; rather, it suggests the presence of an H14 fold and indicates potential self-aggregation.[3a]

Considering **3**, the protic amide protons disappeared immediately after dissolution, suggesting the formation of an extended, strand-like conformation.[4e]

To gain high-resolution structural data, various NMR measurements, including COSY, TOCSY, and ROESY, in 4 mM CD_3OD, DMSO-d_6, and water (90% H_2O + 10% D_2O) solutions were carried out at 297K. Full signal assignment for backbone protons was carried out for **1** and **2**, and long-range NOEs specific for helical β-peptide secondary structures were detected. The long-range NOEs are shown in **Figure 2**

For **1**, long-range NOEs were found typical for H12 helices[4c] in 4 mM concentration in CD_3OD, DMSO-d_6, and water (90% H_2O + 10% D_2O) such as $H_N(4)$–$H_\beta(1)$, $H_N(5)$–$H_\beta(2)$, and $H_\alpha(5)$–$H_\beta(2)$. These NOE crosspeaks are unambiguous signs for the formation of H12 helix. Importantly, the structure tends to be stable in methanol, water, and even in chaotropic DMSO too at 4 mM concentration. The results suggest that the previously known H12 helix made by the homochiral pentamer of [1*S*,2*S*]-ACPC is maintained, that is, betaine conjugation does not influence the helix-forming property of H12.

For **2**, a different set of long-range NOEs was observed in a 4 mM concentration in CD_3OD, DMSO-d_6, and water (90% H_2O + 10% D_2O): $H_N(1)$–$H_\beta(4)$; $H_\alpha(1)$–$H_\beta(4)$, and CH_2(betaine) – $H_\beta(3)$. These long-range interactions were found in 4 mM concentration for the solvents as follows: CD_3OD, DMSO-d_6, and water (90% H_2O + 10% D_2O). This NOE crosspeak pattern is typical to the H14 helix.[3a,4c] These results suggest that in this case the betaine influences the prevailing secondary structure. Namely, the H14 helix is formed rather than the H10 helix published previously.

However, for **3,** the signal dispersion was considerably low; thus, the backbone signal assignment could not be carried out, and it ruled out to look for long-range NOEs to detect a prevailing secondary structure. The low signal dispersion is a considerable sign for strand-like secondary structure formation.[4a,4e] Importantly, due to the introduction of the charged quaternary ammonium ion group of the betaine moiety, compound **3** was soluble in CD_3OD, DMSO-d_6, and water (90% H_2O + 10% D_2O) in a 4 mM concentration too. This opened the way for the utilization of further structure characterization techniques.

To further support the structure characterization data, electronic circular dichroism (ECD) measurements were carried out in methanol and water at a concentration of 1 mM at room temperature (**Figure 3**).

The ECD curve of **1** shows a minor positive band at around 226 nm, while a considerable negative band can be observed at 200 nm in methanol solution. These data are typical for a right-handed helical structure. Considering the NMR data, the most probable secondary is the H12 helix.[4c] In aqueous solution,

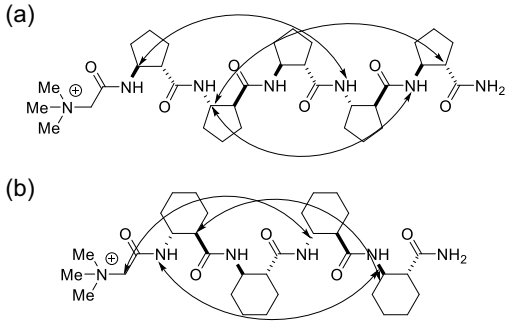

Figure 2. Long-range NOE interactions for 1 a) in DMSO-d6, and for 2 b) found in DMSO-d6, CD3OH or water (90% H2O + 10% D2O).

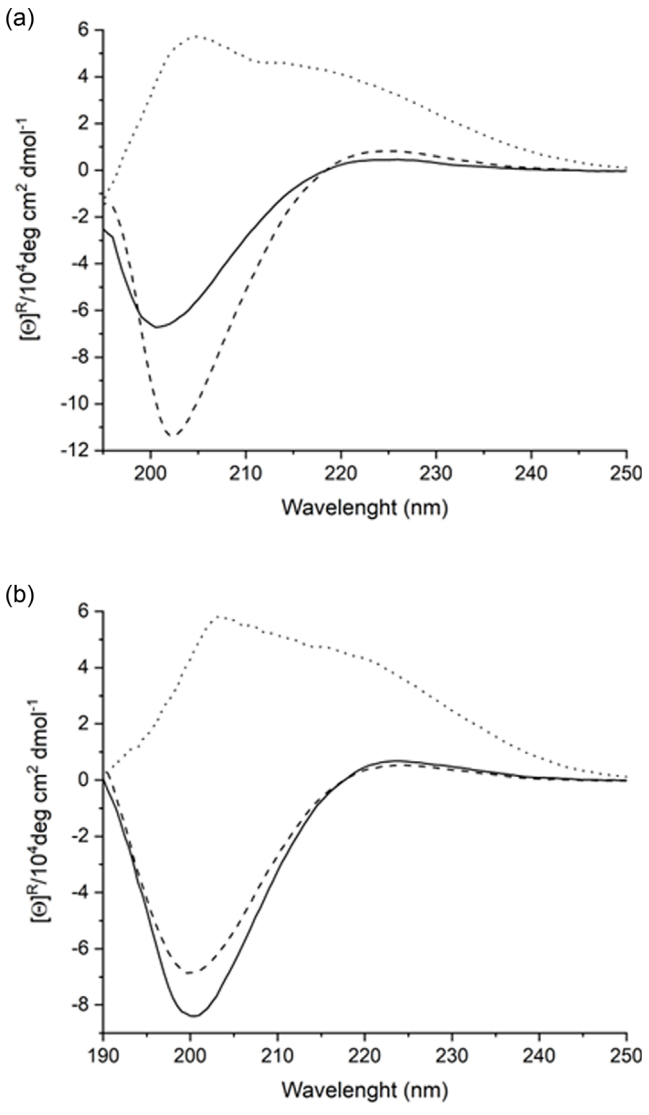

Figure 3. ECD curves of 1 mM solutions of **1** (solid), **2** (dashed) and **3** (dotted) in methanol a) and in water b). Intensities were normalized for the number of chromophores.

the same low-intensity positive band is maintained at 223 nm. However, the intensity of the negative band considerably increased at 201 nm compared to those of methanol solutions. These data suggest that the same helical is maintained in water too. Surprisingly, the stability of the helix increased. This fact points to a potential solvent driven self-association.

For compound **2,** there is positive band at 225 nm and a negative band of higher intensity at 202 nm in methanol. These slight bathochromic shift suggest the presence of a more compact helical fold; thus, the ECD curve indicates the formation of a compact helical conformation. Taking into account the NMR data, the H14 helix formation is most considered in methanol solution.[4c] In water solution, the positive band of compound **2** appears at 224 nm, and the negative band moves to 200 nm. In this case, however, the intensity is considerably lower than those in the methanol solution. This pattern further supports the formation of the same helical structure than those for methanol solution, while it can be stated that the solvent influences the shape of the CD curve. The origin of these minor changes in the CD curve might indicate the potential self-association of the formed helices.

The ECD curve measured for **3** shows a completely different pattern. Importantly, the curve is not crossing the *x* axis, which is a considerable sign for strand-like structure formation.[4c] The curve measured in methanol exhibits positive bands at 212 nm and at 204 nm. A similar pattern can be observed in water, while the intensity of the bands in both solutions tends to be the same. Thus, it can be concluded that the solvent does not have any drastic influence on the prevailing self-organization of the strand-like structure. The introduction of the quaternary charge, by the conjugation of betaine to β-peptide, contributed to water and methanol soluble compound, where ECD curves could be gained from both solvents.

These conformational alterations were also detected by FT-IR spectroscopy. The amide I band is originating mainly from carbonyl stretching vibrations of the peptide backbone.

The most intense band of the deconvoluted amide I of **1** (**Figure 4**a) is $\approx$1641 cm^{-1} which could be assigned to strong intramolecular hydrogen bonds.[3a,4c] This fact supports the helical self-association of the peptide. The two shoulders $\approx$ 1685 cm^{-1} and 1667 cm^{-1} can be related to weaker hydrogen bonds, like the C-terminal amide bond. According to our knowledge, no FT-IR spectrum is available for the H12 helix; however, the gained results underline the formation of a stable helical conformation.

In case of **2**, the deconvoluted amide band show characteristics vibrations of C = O groups $\approx$1646, 1674, and 1690 cm^{-1} involved or not in H-bonding, respectively. This finding supports the results gained by NMR measurements that the conjugation of the betaine unit shifts the folding of peptide to an H14 helix, instead of the expected H10 helices.

In contrast, for **3,** the spectral pattern shows somewhat a different behavior. The sharper band $\approx$1643 cm^{-1} with the presence of a shoulder $\approx$1690 cm^{-1} can also be assigned to stronger and weaker hydrogen bonds involved in peptide folding. The shoulder $\approx$1611 cm^{-1} suggests the presence of intermolecular

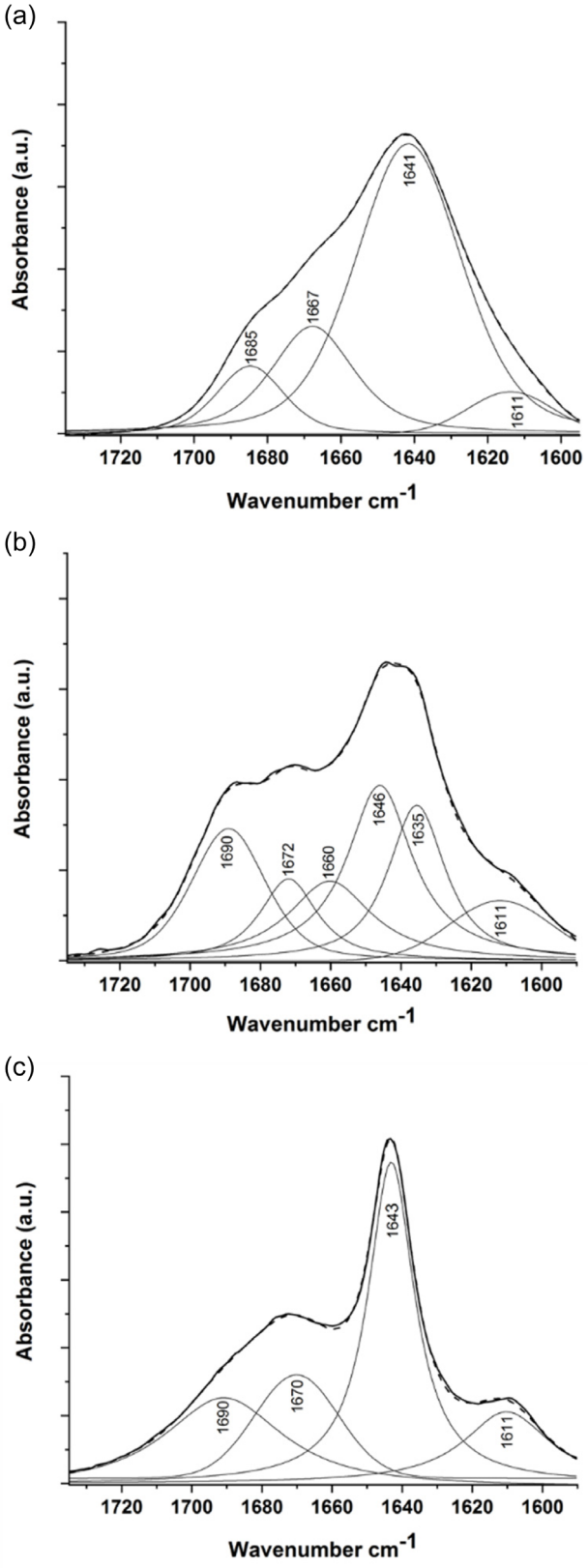

Figure 4. FT-IR spectra in the amide I region of **1** a), **2** b), and **3** c). Spectra were recorded for dry film samples from 1 mM peptide solution and normalized by the area. The solid and dash lines denote the measured and the fitted curves, respectively, whereas thin curves correspond to individual band components (using second derivative IR spectra and Fourier self deconvolution).

hydrogen bonds between β-sheets[18] supporting the formation of strand-like structure.

The extremely prolonged NH/ND exchange observed for **2** and the FT-IR results obtained for **3** indicate the potential self-association of the betaine-conjugated β-peptides. Consequently, transmission electron microscopy (TEM) was used to analyze the self-association phenomena in water solution at 4 mM concentration. The images were recorded after dissolution and sonication (**Figure 5**).

Surprisingly, for helix-forming oligomers **1** and **2,** vesicle formation was observed even in water as solvent.[3a,4c,4d,6g,6h] Importantly, this is the first observation of an H12 helix-forming β-peptide to show self-association in the form of vesicles. The size of the vesicles is in the range of 130–200 nm as shown in Figure 5a.

Importantly, compound **1**, which adopts an H12 helical conformation, was found to self-associate into vesicles with diameters ranging from 130 to 180 nm (Figure 5a). To the best of our knowledge, this represents the first observation of vesicle formation from H12 helical structures. In the case of compound **2**, vesicles with an average diameter similar than those of for **1** were observed (Figure 5b). Notably, there was no need for a time-consuming incubation period, since vesicles were detected immediately after dissolution and sonication. This observation further supports the view that by the introduction of quaternary positive charges the vertical amphiphilicity of β-peptides can be increased, resulting in higher tendency for self-association manifesting in vesicle formation. These results suggest that by betaine conjugation not only the secondary structure, but the formation of tertiary structural element formation can be fine-tuned. Importantly, the self-association was found in water, which is a considerably more biorelevant solvent.

The TEM images recorded for **3** showed a significantly different pattern (Figure 5c). Vesicle formation was not observed, rather, nanosized fibrils were found. This result is in accordance with literature data. For example, peptides forming strand-like secondary structure have strong propensity for nanosized fibril formation.[4d,4e] Note, however, that this is the first observation for the formation of a β-peptide fibril formation in aqueous medium. Moreover, the observed fibrils form a concatenated fibrinous net-like structure.

To further support the previously gained experimental results, theoretical calculations were carried out. Quantum mechanical DFT (density functional theory) calculations, namely geometry optimizations, were carried out at the B3LYP/6-311G** level of theory with the Jaguar software package.[19] The calculations suggest the formation of an H12 helix for **1** and an H14 helix for **2**. For **3**, the calculation supported the formation of an antiparallel β-sheet formation by the self-association of E-strands. The optimized geometries are shown in **Figure 6**.

It can be concluded that betaine conjugation significantly influenced the folding, self-assembly, and solubility of a set of β-peptide foldamers. The oligomers were synthetized on solid support by the use of a prominently economic continuous-flow technology, which allowed the use of only 1.5-fold of excess of amino acids.

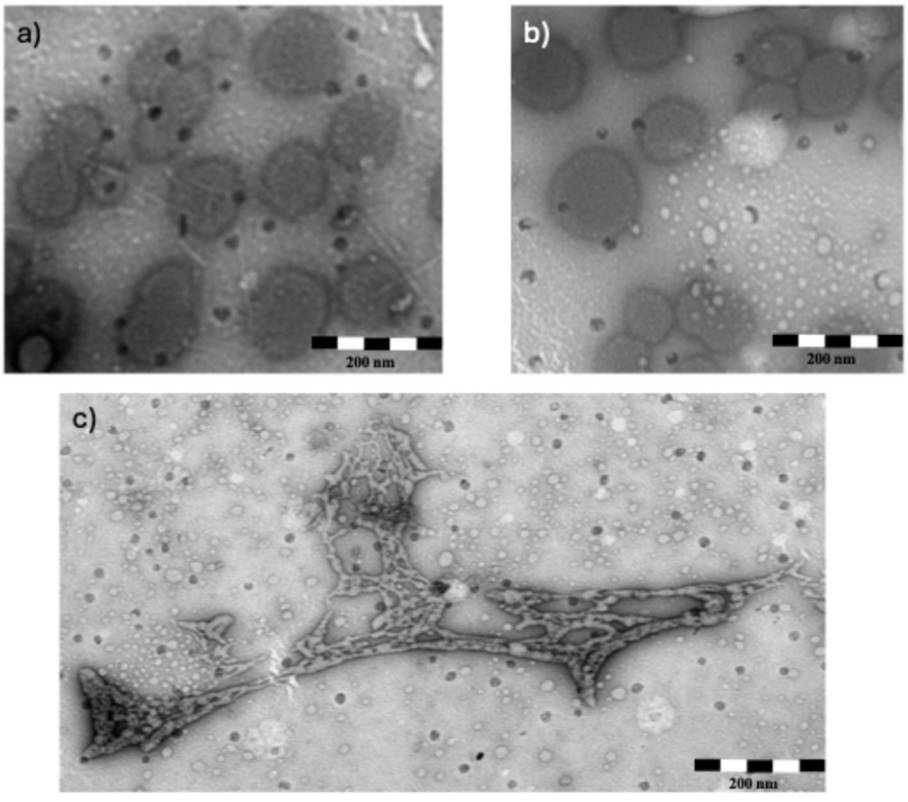

Figure 5. TEM images of vesicles observed after dissolution and sonication of 4 mM solutions of **1** a), **2** b), and **3** c) in water.

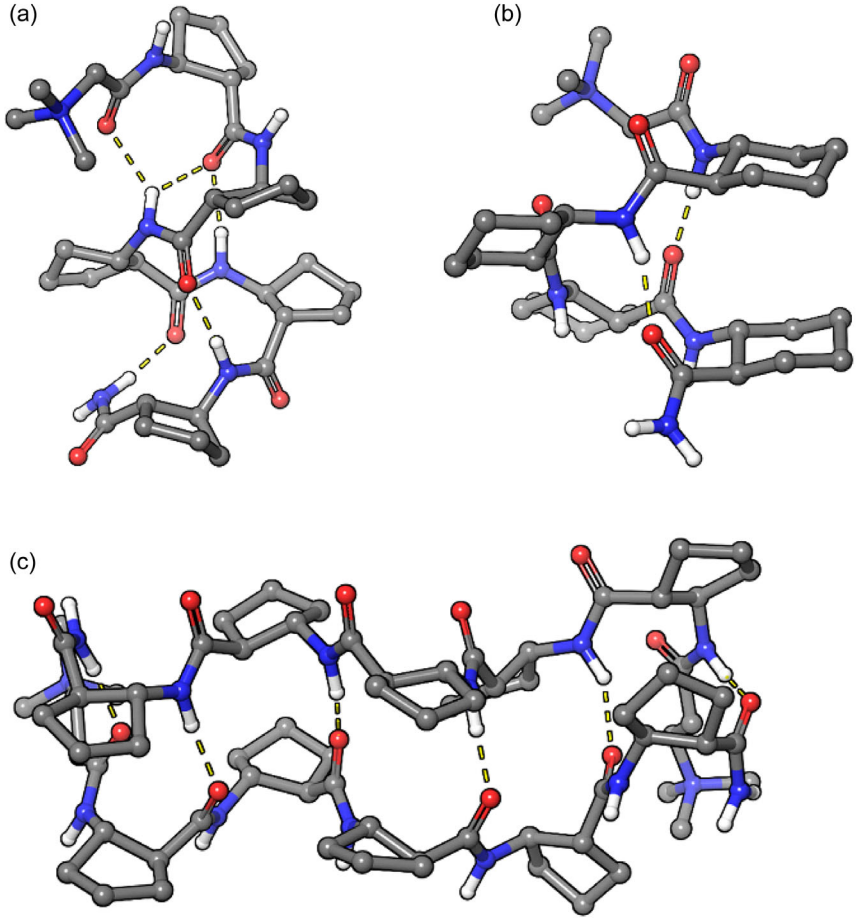

Figure 6. Optimized ab initio geometry of **1** a), **2** b), and **3** c) at the B3LYP/6-311G** level of theory.

In the case of the [1*S*,2*S*]-ACPC pentamer (**1**), betaine conjugation did not influence the folding of an H12 helix. However, the self-association of this oligomer was considerably facilitated. In water as solution, vesicles in the range of 130−180 nm were observed in TEM images.

For the [1*R*,2*R*]-ACHC tetramer (**2**), betaine conjugation significantly influenced the folding. Note, however, that formation of the H14 helix was observed instead of the expected H10 helix. Betaine conjugation considerably increased the self-association property, and immediately after dissolution and sonication, vesicles with a diameter of ca. 200 nm were observed in TEM images.

For the alternating heterochiral [1*S*,2*S*]-ACPC and [1*R*,2*R*]-ACPC pentamer (**3**), betaine conjugation increases the solubility of the system. The prevailing secondary structure is the expected E-strand, which is capable of self-association in the form of amyloid like fibrils. However, betaine conjugation modified slightly this behavior, and a concatenated, fibrin net-like structure was observed.

For the investigated betaine-conjugated oligomers, self-association was found in aqueous medium. This fact opens the window for biomedical and material chemical utilization of β-peptide foldamers containing alicyclic side-chain.

3. Experimental Section

Peptide Synthesis

Peptide chains were extended on a Tentagel R RAM resin (0.20 mmol g^{-1}). For CF experiments, a modular CF apparatus was assembled, consisting of a cylindrical PEEK column (with internal dimensions of 250 × 4 mm) filled with the resin-loaded amino acid (350 mg), a semipreparative pump (JASCO PU-4086), an HPLC autosampler (JASCO AS-4150), a column oven (JASCO CO-4060), two line-selecting valve units (JASCO HV-4380), and a backpressure regulator. A coupling mixture, consisting of 1.5 equivalents of Fmoc-protected β-amino acid and 1.5 equivalents of OxymaPure as coupling reagent dissolved in DMF and 1.5 equivalents of DIC, was mixed by the autosampler. The coupling mixture has been prepared immediately before the coupling reaction. Coupling reactions were carried out at the optimized reaction conditions, 85 bar pressure, 65 °C temperature, and 0.2 mL min^{-1} flow rate. For Fmoc deprotection, the solution of 2 mL of 2% DBU 2% piperidine in DMF has been used. Between two chemical steps DMF was used for washing for 5 min.

NMR Experiments

NMR measurements for signal assigment were carried out on a Bruker Avance III 500 MHz spectrometer equipped with a cryo probe head. Peptide samples (4 mM) were prepared in H_2O/D_2O 90:10 v/v,

DMSO-d_6, or CD_3OH and transferred into 5 mm NMR sample tubes. For the ROESY spinlock, a mixing time of 300 ms was used; the number of scans was 16, and roesyesgpph or roesyph.2 (DMSO-d_6) pulse sequence was applied. The TOCSY measurement was performed with the mlevesgpph or mlevph (DMSO-d_6) sequence, with a mixing time of 150 ms; the number of scans was 16. For all 2D spectra, 4k time domain points and 512 increments were applied. T2 relaxation experiments were carried out by cpmg_esgp2d or cpmg (DMSO-d_6) pulse sequence; the relaxation delays were incremented in the following order: 1, 2, 4, 8, 16, 32, 64, 128, 256, 512, and 1024 ms.

The NH/ND exchange was recorded on a Varian Mercury 400 spectrometer equipped with ATB PFG probe head. The samples were prepared in 4 mM concentration in CD_3OD and transferred into standard 5 mm NMR sample tubes. The recording was started 10 min after complete solubilization. The ^1H spectra were recorded using 64 scans with 45° pulse and 5 s relaxation delay.

CD Measurements

CD spectra were measured on a Jasco J-1500 spectropolarimeter at 25°C in a 0.1 cm path length regtangular quartz cuvette (Hellma, Plainview, NY) in a continuous scanning mode between 190 and 250 nm at a rate of 50 nm min^{-1}, with a data pitch of 0.5 nm, a response time of 4 s, a 1 nm bandwidth, and 3 times accumulation for each sample. The baseline spectrum recorded with the solvent was subtracted from the raw data. The concentration of the sample solutions in ultrapure water and PBS was 1 mM. Molar circular dichroism is given in $mol^{-1}\,cm^{-1}$.

ATR-FTIR Measurement

A Varian 2000 FTIR Scimitar spectrometer (Varian Inc., Palo Alto, CA) was used for FTIR spectroscopic measurements. The spectrometer is fitted with a liquid nitrogen-cooled mercury-cadmium-telluride (MCT) detector with a 'Golden Gate' single reflection diamond ATR accessory (Specac Ltd., Orpington, U.K.). On the diamond ATR surface, 3 µL of the sample was mounted, and the spectrum was accumulated (2 cm^{-1} resolution and 64 scans) for the dry film after gradual evaporation of the buffered solvent under ambient conditions. ATR correction for every data acquisition, buffer subtraction, and baseline corrections were performed. The GRAMS/32 software package (Galactic Inc.) was used for all spectral manipulations.

TEM Measurement

The peptides were dissolved in water to a concentration of 1 mM, and the solution was sonicated for 5 min. Drops of 5 µL of solutions were placed onto Formvar-coated 200-mesh copper grids (Ted Pella Inc, USA) and dried in the air at 25°C for 10 min. Specimens were studied with a MORGAGNI 268D transmission electron microscope (FEI, Eindhoven, The Netherlands) operated at 80 kV and equipped with a Quemesa 11-megapixel bottom-mounted CCD camera (Emsis GmbH, Germany).

Model Building and Theoretical Calculations

The structures were drawn with Schrödinger's Maestro 2D Sketcher, the hydrogen atoms were added, and the structures were quickly optimized into 3D geometry. A conformational search for each compound was completed with the MacroModel package 'Energy minimization' option using the OPLS4 force field with 'no solvent' option with the default settings. In the case of dimer **3**, in order to maintain the interaction between the two chains, 'frozen' atom constraints were applied on the corresponding hydrogen and oxygen atoms participating in the H-bonds. The output structures of the minimization of each compound were used as initial geometries for further calculations.

The Jaguar geometry optimization calculations were completed in two steps. First, the Restricted Hartree–Fock (RHF) method was applied with 3-21G basis set in a vacuum. Second, the density functional theory (DFT) method (B3LYP-D3 functional) was applied with 6-311G** basis set in vacuum. In the case of dimer **3**, implicit water was necessary in order to maintain chain-like conformation, and the polarizable continuum model (PCM) solvation model was applied.

The software packages as follows were used: Maestro (v13.8): Release 2023-4, Schrödinger, LLC, New York, NY, 2023; MacroModel (v14.2): Release 2023-4, Schrödinger, LLC, New York, NY, 2023; and Jaguar (v12.2): Release 2023-4, Schrödinger, LLC, New York, NY, 2023.

Acknowledgements

We are grateful to the Hungarian Research Foundation (OTKA ANN 139484). The financial support of the National Research, Development and Innovation Office (TKP2021-EGA-31) is acknowledged. Project no. RRF-2.3.1-21-2022−00015 has been implemented with support provided by the European Union. E.E. acknowledges the grant of EFOP-3.6.3-VEKOP-16-2017−00009.

Conflict of Interest

The authors declare no conflict of interest.

Data Availability Statement

The data that support the findings of this study are available in the supplementary material of this article.

Keywords: ß-amino acid · betaine · folding · peptide · quaternary charge

[1] a) P. S. P. Wang, A. Schepartz, *Chem. Commun.* **2016**, *52*, 7420; b) K. Kulkarni, N. Habila, M. P. D. Borgo, M.-I. Aguilar, *Front. Chem.* **2019**, *7*, e70; c) R. D. Gopalan, M. P. D. Borgo, A. I. Mechler, P. Perlmutter, M.-I. Aguilar, *Chem. Biol.* **2015**, *22*, 1417; d) I. M. Mándity, F. Fülöp, *Expert Opin. Drug Discov.* **2015**, *10*, 1163; e) A. Schepartz, *Nat. Chem.* **2018**, *10*, 377; f) P. M. D. Borgo, K. Kulkarni, M.-I. Aguilar, *Curr. Pharm. Des.* **2017**, *23*, 3772; g) D. Seebach, J. Gardiner, *Acc. Chem. Res.* **2008**, *41*, 1366; h) M. P. D. Borgo, K. Kulkarni, M. A. Tonta, J. L. Ratcliffe, R. Seoudi, A. I. Mechler, P. Perlmutter, H. C. Parkington, M.-I. Aguilar, *APL Bioeng.* **2018**, *2*, 026104.

[2] a) D. H. Appella, L. A. Christianson, I. L. Karle, D. R. Powell, S. H. Gellman, *J. Am. Chem. Soc.* **1996**, *118*, 13071; b) S. H. Gellman, *Acc. Chem. Res.* **1998**, *31*, 173.

[3] a) A. Hetenyi, I. M. Mandity, T. A. Martinek, G. K. Toth, F. Fulop, *J. Am. Chem. Soc.* **2005**, *127*, 547; b) R. P. Cheng, S. H. Gellman, W. F. DeGrado, *Chem. Rev.* **2001**, *101*, 3219; c) M.-r. Lee, T. L. Raguse, M. Schinnerl, W. C. Pomerantz, X. Wang, P. Wipf, S. H. Gellman, *Org. Lett.* **2007**, *9*, 1801; d) E. Abraham, C. W. Bailey, T. D. W. Claridge, S. G. Davies,

K. B. Ling, B. Odell, T. L. Rees, P. M. Roberts, A. J. Russell, A. D. Smith, L. J. Smith, H. R. Storr, M. J. Sweet, A. L. Thompson, J. E. Thomson, G. E. Tranter, D. J. Watkin, *Tetrahedron: Asymmetry* **2010**, *21*, 1797.

[4] a) T. A. Martinek, G. K. Toth, E. Vass, M. Hollosi, F. Fulop, *Angew. Chem.-Int. Edit.* **2002**, *41*, 1718; b) T. A. Martinek, F. Fulop, *Eur. J. Biochem.* **2003**, *270*, 3657; c) F. Fulop, T. A. Martinek, G. K. Toth, *Chem. Soc. Rev.* **2006**, *35*, 323; d) T. A. Martinek, A. Hetenyi, L. Fulop, I. M. Mandity, G. K. Toth, I. Dekany, F. Fulop, *Angew. Chem.-Int. Edit.* **2006**, *45*, 2396; e) T. A. Martinek, I. M. Mandity, L. Fulop, G. K. Toth, E. Vass, M. Hollosi, E. Forro, F. Fulop, *J. Am. Chem. Soc.* **2006**, *128*, 13539.

[5] a) T. A. Martinek, F. Fulop, *Chem. Soc. Rev.* **2012**, *41*, 687; b) R. P. Cheng, S. H. Gellman, W. F. DeGrado, *Chem. Rev.* **2001**, *101*, 3219; c) X. Daura, K. Gademann, H. Schäfer, B. Jaun, D. Seebach, W. F. van Gunsteren, *J. Am. Chem. Soc.* **2001**, *123*, 2393; d) D. Seebach, S. Abele, K. Gademann, B. Jaun, *Angew. Chem. Int. Ed.* **1999**, *38*, 1595.

[6] a) M. W. Giuliano, W. S. Horne, S. H. Gellman, *J. Am. Chem. Soc.* **2009**, *131*, 9860; b) W. S. Horne, *Nat Chem* **2015**, *7*, 858; c) D. S. Daniels, E. J. Petersson, J. X. Qiu, A. Schepartz, *J. Am. Chem. Soc.* **2007**, *129*, 1532; d) J. L. Goodman, E. J. Petersson, D. S. Daniels, J. X. Qiu, A. Schepartz, *J. Am. Chem. Soc.* **2007**, *129*, 14746; e) J. L. Goodman, M. A. Molski, J. Qiu, A. Schepartz, *ChemBioChem* **2008**, *9*, 1576; f) G. L. Montalvo, Y. Zhang, T. M. Young, M. J. Costanzo, K. B. Freeman, J. Wang, D. J. Clements, E. Magavern, R. W. Kavash, R. W. Scott, D. Liu, W. F. DeGrado, *Acs Chem. Biol.* **2014**, *9*, 967; g) I. M. Mandity, L. Fulop, E. Vass, G. K. Toth, T. A. Martinek, F. Fulop, *Org. Lett.* **2010**, *12*, 5584; h) I. M. Mándity, A. Monsignori, L. Fülöp, E. Forró, F. Fülöp, *Chem. Eur. J.* **2014**, *20*, 4591; i) I. M. Mándity, I. Nekkaa, G. Paragi, F. Fülöp, *ChemistryOpen*, **2017**, *6*, 492.

[7] a) C. M. Rufo, Y. S. Moroz, O. V. Moroz, J. Stöhr, T. A. Smith, X. Hu, W. F. DeGrado, I. V. Korendovych, *Nat. Chem.* **2014**, *6*, 303; b) I. C. Szigyártó, J. Mihály, A. Wacha, D. Bogdán, T. Juhász, G. Kohut, G. Schlosser, F. Zsila, V. Urlacher, Z. Varga, F. Fülöp, A. Bóta, I. Mándity, T. Beke-Somfai, *Chem. Sci.* **2020**, *11*, 6868; c) M. P. D. Borgo, A. I. Mechler, D. Traore, C. Forsyth, J. A. Wilce, M. C. J. Wilce, M.-I. Aguilar, P. Perlmutter, *Angew. Chem. Int. Ed.* **2013**, *52*, 8266; d) A. J. Christofferson, Z. S. Al-Garawi, N. Todorova, J. Turner, M. P. D. Borgo, L. C. Serpell, M.-I. Aguilar, I. Yarovsky, *ACS Nano* **2018**, *12*, 9101; e) K. Luder, K. Kulkarni, H. W. Lee, R. E. Widdop, M. P. D. Borgo, M.-I. Aguilar, *Chem. Commun.* **2016**, *52*, 4549; f) T. A. Martinek, I. M. Mándity, L. Fülöp, G. K. Tóth, E. Vass, M. Hollósi, E. Forró, F. Fülöp, *J. Am. Chem. Soc.* **2006**, *128*, 13539.

[8] a) G. Guichard, I. Huc, *Chem. Commun.* **2011**, *47*, 5933; b) C. Mayer, M. M. Müller, S. H. Gellman, D. Hilvert, *Angew. Chem. Int. Ed.* **2014**, *53*, 6978; c) S. Kwon, A. Jeon, S. H. Yoo, I. S. Chung, H.-S. Lee, *Angew. Chem. Int. Ed.* **2010**, *49*, 8232; d) J. W. Checco, E. F. Lee, M. Evangelista, N. J. Sleebs, K. Rogers, A. Pettikiriarachchi, N. J. Kershaw, G. A. Eddinger, D. G. Belair, J. L. Wilson, C. H. Eller, R. T. Raines, W. L. Murphy, B. J. Smith, S. H. Gellman, W. D. Fairlie, *J. Am. Chem. Soc.* **2015**, *137*, 11365; e) G. Marafon, M. Crisma, A. Masato, N. Plotegher, L. Bubacco, A. Moretto, *Angew. Chem. Int. Ed.* **2021**, *60*, 5173; f) B. Nizami, D. Bereczki-Szakál, N. Varró, K. el Battioui, V. U. Nagaraj, I. C. Szigyártó, I. Mándity, T. Beke-Somfai, *Nucleic Acids Res.* **2019**, *48*, D1122; g) K. el Battioui, S. Chakraborty, A. Wacha, D. Molnár, M. Quemé-Peña, I. C. Szigyártó, C. L. Szabó, A. Bodor, K. Horváti, G. Gyulai, S. Bősze, J. Mihály, B. Jezsó, L. Románszki, J. Tóth, Z. Varga, I. Mándity, T. Juhász, T. Beke-Somfai, *Nat. Commun.* **2024**, *15*, 3424.

[9] a) A. Davenport, C. Scully, C. de Graaf, A. Brown, J. Maguire, *Nat. Rev. Drug Discov.* **2020**, *1*, 389. b) É. Bartus, Z. Hegedüs, E. Wéber, B. Csipak, G. Szakonyi, T. A. Martinek, *Chemistryopen* **2017**, *6*, 236. c) J. W. Checco, S. H. Gellman, *Curr. Opin. Struct. Biol.* **2016**, *39*, 96.

[10] a) P.-N. Cheng, C. Liu, M. Zhao, D. Eisenberg, J. S. Nowick, *Nat. Chem.* **2012**, *4*, 927; b) J. W. Checco, D. F. Kreitler, N. C. Thomas, D. G. Belair, N. J. Rettko, W. L. Murphy, K. T. Forest, S. H. Gellman, *Proc. Natl. Acad. Sci.* **2015**, *112*, 4552; c) H. S. Haase, K. J. Peterson-Kaufman, S. K. L. Levengood, J. W. Checco, W. L. Murphy, S. H. Gellman, *J. Am. Chem. Soc.* **2012**, *134*, 7652; d) Z. Hegedüs, E. Wéber, É. Kriston-Pál, I. Makra, Á. Czibula, É. Monostori, T. A. Martinek, *J. Am. Chem. Soc.* **2013**, *135*, 16578.

[11] a) P. S. P. Wang, J. B. Nguyen, A. Schepartz, *J. Am. Chem. Soc.* **2014**, *136*, 6810; b) G. Maayan, M. D. Ward, K. Kirshenbaum, *Proc. Natl. Acad. Sci.* **2009**, *106*, 13679; c) M. M. Müller, M. A. Windsor, W. C. Pomerantz, S. H. Gellman, D. Hilvert, *Angew. Chem. Int. Ed.* **2009**, *48*, 922.

[12] a) M. S. Melicher, A. S. Walker, J. Shen, S. J. Miller, A. Schepartz, *Org. Lett.* **2015**, *17*, 4718; b) M. S. Melicher, J. Chu, A. S. Walker, S. J. Miller, R. H. G. Baxter, A. Schepartz, *Org. Lett.* **2013**, *15*, 5048.

[13] a) I. M. Mandity, E. Weber, T. A. Martinek, G. Olajos, G. K. Toth, E. Vass, F. Fulop, *Angew. Chem., Int. Ed.* **2009**, *48*, 2171; b) Ł. Berlicki, L. Pilsl, E. Wéber, I. M. Mándity, C. Cabrele, T. A. Martinek, F. Fülöp, O. Reiser, *Angew. Chem. Int. Ed.* **2012**, *51*, 2208; c) I. Nekkaa, D. Bogdán, T. Gáti, S. Béni, T. Juhász, M. Palkó, G. Paragi, G. K. Tóth, F. Fülöp, I. M. Mándity, *Chem. Commun.* **2019**, *55*, 3061.

[14] a) A. Hetenyi, Z. Szakonyi, I. M. Mandity, E. Szolnoki, G. K. Toth, T. A. Martinek, F. Fulop, *Chem. Commun.* **2009**, 177; b) A. Hetényi, G. K. Tóth, C. Somlai, E. Vass, T. A. Martinek, F. Fülöp, *Chem. Eur. J.* **2009**, *15*, 10736; c) E. Szolnoki, A. Hetenyi, I. M. Mandity, F. Fulop, T. A. Martinek, *Eur. J. Org. Chem.* **2013**, 3555; d) F. Rua, S. Boussert, T. Parella, I. Diez-Perez, V. Branchadell, E. Giralt, R. M. Ortuno, *Org. Lett.* **2007**, *9*, 3643; e) E. Torres, E. Gorrea, K. K. Burusco, E. Da Silva, P. Nolis, F. Rua, S. Boussert, I. Diez-Perez, S. Dannenberg, S. Izquierdo, E. Giralt, C. Jaime, V. Branchadell, R. M. Ortuno, *Org. Biomol. Chem.* **2010**, *8*, 564; f) M. Alauddin, E. Gloaguen, V. Brenner, B. Tardivel, M. Mons, A. Zehnacker-Rentien, V. Declerck, D. J. Aitken, *Chem. Eur. J.* **2015**, *21*, 16479; g) C. M. Grison, J. A. Miles, S. Robin, A. J. Wilson, D. J. Aitken, *Angew. Chem. Int. Ed.* **2016**, *55*, 11096; h) C. M. Grison, S. Robin, D. J. Aitken, *Chem. Commun.* **2016**, *52*, 7802; i) S. S. Ragab, A. F. Kassir, R. Guillot, M.-C. Scherrmann, T. Boddaert, D. J. Aitken, *Chem. Commun.* **2018**, *54*, 1968.

[15] a) A. Boto, C. C. González, D. Hernández, I. Romero-Estudillo, C. J. Saavedra, *Org. Chem. Front.* **2021**, *8*, 6720; b) Y. Li, K. A. Clark, Z. Tan, *Chin. Chem. Lett.* **2018**, *29*, 1074; c) J. Sun, F. Zeng, H. Jian, S. Wu, *Biomacromolecules* **2013**, *14*, 728; d) J. Xiao, A. Burn, T. J. Tolbert, *Bioconjugate Chem.* **2008**, *19*, 1113;

[16] D. H. Appella, L. A. Christianson, D. A. Klein, D. R. Powell, X. L. Huang, J. J. Barchi, S. H. Gellman, *Nature* **1997**, *387*, 381.

[17] a) I. M. Mándity, B. Olasz, S. B. Ötvös, F. Fülöp, *ChemSusChem* **2014**, *7*, 3172; A. Szloszár, F. Fülöp, I. M. Mándity, *ChemistrySelect***2017**, *2*, 6036; c) A. Szloszár, I. M. Mándity, F. Fülöp, *J. Flow Chem.* **2018**, *8*, 21.

[18] A. Sadat, I. J. Joye, *Appl. Sci.* **2020**, *10*, 5918.

[19] A. D. Bochevarov, E. Harder, T. F. Hughes, J. R. Greenwood, D. A. Braden, D. M. Philipp, D. Rinaldo, M. D. Halls, J. Zhang, R. A. Friesner, *Int. J. Quantum Chem.* **2013**, *113*, 2110.

Manuscript received: June 20, 2025
Revised manuscript received: September 15, 2025
Version of record online: September 27, 2025